Review of Materials Research 1 (2025) 100015

Contents lists available at ScienceDirect

Review of Materials Research

journal homepage: www.sciencedirect.com/journal/review-of-materials-research

High thermal stability chalcogenide phase-change materials for embedded memory applications

Ruobing Wang [a], Ziqi Wan [a,b], Xixi Zou [a,c], Shanwen Chen [a,b], Sannian Song [a], Xilin Zhou [a,*], Zhitang Song [a]

[a] State Key Laboratory of Materials for Integrated Circuits, Shanghai Institute of Microsystem and Information Technology, Chinese Academy of Sciences, Shanghai, 200050, China

[b] University of Chinese Academy of Sciences, Beijing, 100049, China

[c] School of Physical Science and Techonlogy, ShanghaiTech University, Shanghai, 201210, China

ARTICLE INFO

Keywords:
Phase-change material
Embedded memory
Thermal stability
GeSbTe

ABSTRACT

Chalcogenide phase-change materials are capable of switching rapidly between a disordered amorphous phase and an ordered crystalline phase, associating with the pronounced differences in electrical and optical properties. The resistance contrast is widely used for data storage in phase-change memories (PCMs). As the most promising emerging non-volatile memory, PCMs have been intensively explored for embedded data storage applications. The key challenge of embedded PCMs (ePCMs) is to realize reliable electrical switching performance in an environment with high thermal budget, in which the thermal stability of chalcogenide phase-change materials is crucial to retain the encoded information. We present a review of the material engineering of chalcogenide phase-change materials by doping to address the high thermal stability challenge. The mechanism of performance optimization and industrial applications of the chalcogenide materials are also included, which are important for the development of ePCMs with high thermal stability and excellent performance.

1. Introduction

The rapid development in information technology has triggered and enabled the fourth industrial revolution with technologies explored in smart car, artificial intelligence, cloud storage, and internet of things. Throughout these applications, an unprecedented amount of data is created, which needs to be collected, processed and stored quickly and reliably. Along with this trend, memory technology has been continuing to innovate to meet the growing demands of data storage, such as high-density three-dimensional NAND flash memories [1] and high bandwidth dynamic random-access memories (DRAMs) [2]. However, due to the large performance gap between the existing semiconductor memories, a "storage wall" caused by the difference in data latency and capacity between DRAM and NAND is recognized, which hinders the further improvement of performance and efficiency of computing [3]. To address the performance gap between DRAM and NAND, storage class memories (SCMs) are proposed with a variable and customizable combination of cost and access latency [4], as shown in Fig. 1. SCMs are supposed to be non-volatile, with shorter latency than NAND and lower cost and higher capacity than DRAM.

Several non-volatile emerging memories have been considered as the candidates for SCMs, such as resistive random-access memory (RRAM), phase-change memory (PCM), and magnetoresistive random-access memory (MRAM). Fig. 2 shows the performances comparison among the existing memory technologies [5], in which PCM has been intensively explored by both academia and industry with a great potential to be used as ePCM and SCM. As the process node goes down to sub-20 nm in emerging memories, PCM has received increasing attention with the advantages of low power and high speed due to the reduced active switching region [6]. In 2015, 3D X-point memory is developed based on chalcogenide materials, which is considered as a revolutionary breakthrough in non-volatile memory technology [7]. Intel applied this technology on the Optane product of solid-state storage drives for stand-alone applications [8]. Besides the stand-alone market, the embedded data storage applications are another major driven for PCM technology due to the physical limits in the highly scaled traditional Flash memory [9]. The embedded application for memory products including micro-controller units (MCUs), automotive, smart cards, and IoT requires high operation temperature [10]. Samsung proposed a 512 Mb diode selected PCM with significantly enhanced cell density [11]. Later in 2010, Samsung

* Corresponding author.
E-mail address: xilinzhou@mail.sim.ac.cn (X. Zhou).

https://doi.org/10.1016/j.revmat.2025.100015
Received 21 March 2025; Received in revised form 6 April 2025; Accepted 6 April 2025
Available online 8 April 2025
3050-9130/© 2025 The Author(s). Published by Elsevier B.V. on behalf of Chinese Materials Research Society. This is an open access article under the CC BY-NC-ND license (http://creativecommons.org/licenses/by-nc-nd/4.0/).

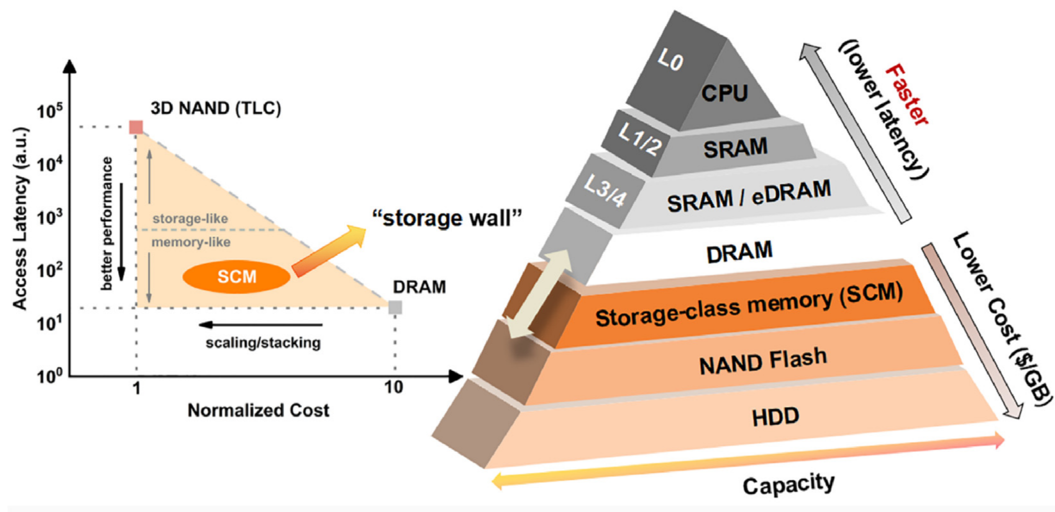

Fig. 1. The position of SCM in the memory hierarchy [4].

Good / Bad / Average	SRAM	DRAM	NAND FLASH	NOR FLASH	FeRAM	RRAM	STT-MRAM	SOT-MRAM	PCM
Cell Size	>150 F^2	6 F^2	<4 F^2 (3D)	10 F^2	6-50 F^2	4-10 F^2	6-50 F^2	12-100 F^2	4-12 F^2
Stackable	NO	YES	YES	YES	NO	YES	NO	NO	YES
MLC	NO	NO	YES (4)	NO	NO	YES	NO	NO	YES (2)
Scaling	< 3nm	~ 10nm	~ 14nm	~ 45nm	< 10nm	< 10nm	< 10nm	< 10nm	< 10nm
Voltage	< 1V	< 1V	> 10V	> 10V	< 2V	< 3V	< 1V	< 1V	< 3V
Latency(R/W)	all 1ns	all 10ns	10/100µs	50ns 100µs	all 100ns	50/100ns	10/20ns	10/3ns	50/100ns
Endurance	> 10^{16}	> 10^{16}	10^4-10^5	10^5	10^9-10^{12}	10^6-10^{11}	10^6-10^{15}	~10^{12}	10^6-10^8
Retention	Volatile	Volatile	>10yr	>10yr	>10yr	>10yr	>10yr	>10yr	>10yr
Write Energy	~fJ	~10fJ	~10fJ	~100pJ	~100fJ	~pJ	~pJ	~pJ	~10pJ

Fig. 2. Performances comparison among tradition semiconductor and emerging non-volatile memories [5].

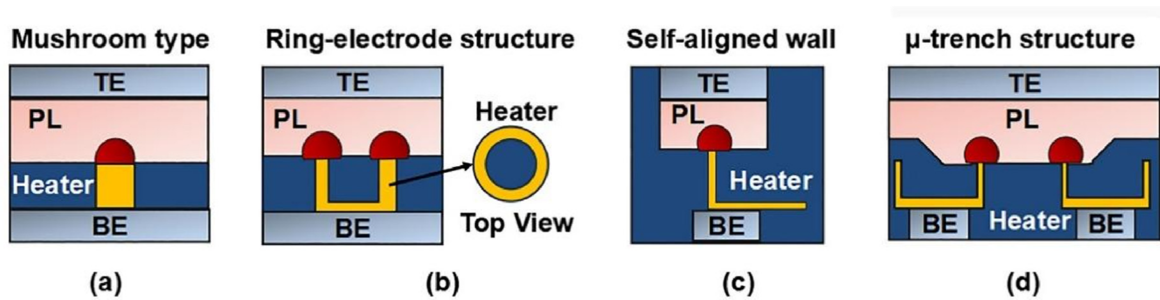

Fig. 3. The cell structure of PCM used in the ePCM. (a) Mushroom type. (b) Ring-electrode structure. (c) Self-aligned wall structure. (d) µ-trench structure. Dielectric areas shown in dark-blue and red areas are the active regions in PCL. Heater is shown in orange, and the grey blocks are top/bottom electrodes.

announced the PCM products for smartphones [12]. In 2018, STMicroelectronics (STM) proposed a 28 nm FDSOI embedded non-volatile memory (eNVM) solution for automotive MCU applications using PCM based on chalcogenide ternary material [55].

Among all resistive memories proposed to replace embedded Flash memory, ePCM is the only one that has been proved to meet the most stringent requirements of the automotive industry [13]. The 10-year data retention temperature (T_{10}) of ePCM is up to 150 °C. ePCM also survives after reflow soldering (curve peak temperature 260 °C) with fast programming, bit alterability, low programming current, as well as sufficient reliability [14]. The switching performance of ePCMs is highly dependent on the device structure. Since the resistance of PCMs is modulated by Joule heat, it is an effective way to increase the heating efficiency by using a passive heater to confine the programming current. The most used heater material is TiN or W and the active region in phase-change material layer (PCL) is expected to form at the interface between the

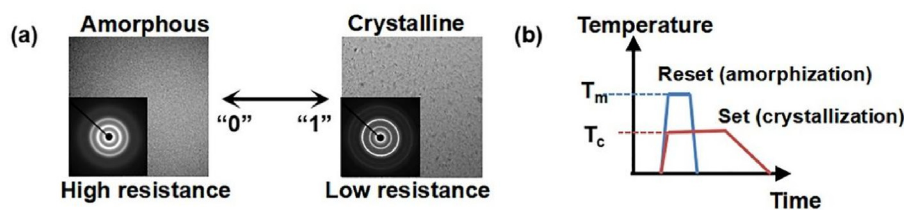

Fig. 4. Reversible phase change mechanism of phase-change materials: (a) Reversible switching between high resistance amorphous phase and low resistance crystalline phase, with the TEM images and SAED inset. (b) The schematic diagram of the Set and Reset pulses.

heater and chalcogenide [15]. Fig. 3 shows four types of device structures used in ePCMs in order to reduce the programming current. The typical mushroom type PCM cell shown in Fig. 3(a) prefers the reduced diameter of the heater for a lower programming current, which, however, induces larger variation in cell resistance [16]. Fig. 3(b) shows the ring-shape electrode structure used to control the heater resistance [17]. To further decrease the programming current, an L-type heater is proposed, which is also known as self-aligned wall structure, as shown in Fig. 3(c) [18]. STM presented a μ-trench structure, as shown in Fig. 3(d), which effectively reduces the programming current with the cost of increased process steps [19]. The self-aligned wall structure is always presented in the ePCM devices by STM [20].

The chalcogenide phase-change material plays a key role in ePCM. The most popular chalcogenide is $Ge_2Sb_2Te_5$ (GST) alloy, which has been used in stand-alone PCM products. However, the low crystallization temperature (T_c) limits its switching performance at high temperature. For eNVM applications, the T_c of phase-change material needs to be at least 50 °C higher than GST. Therefore, the development of high thermal stable chalcogenide phase-change material is crucial for ePCMs. This paper provides a review of the material engineering of high thermal stable phase-change materials for embedded data storage applications. The performances of the optimized phase-change material will be presented, followed by the discussion of switching mechanisms. The performance ePCM chips will also be addressed followed by the introduction of challenge and prospect of phase-change material.

2. Phase-change material

The discovery of a transition between high and low resistance levels in chalcogenide compounds under electric field excitation was reported by Ovshinsky in 1968 [21]. The amorphous state of chalcogenide phase-change materials has high resistance, corresponding to logic state "0". If a long pulse of low amplitude is applied, the material will be affected by the heat generated by the electric pulse and transform from the amorphous to crystalline state with low resistance (corresponding to logic state "1″). This crystallization process is called Set programming, which is related to T_c of the phase-change material. When applying a short electrical pulse with sufficient energy to the crystallized material, the material will be melt-quenched to the amorphous state of high resistance. The amorphization process is called Reset programming, which is affected by the melting temperature (T_m) of phase-change material. The corresponding schematic diagram of the fast reversible switching between the two phases is shown in Fig. 4.

The earlier publications on phase-change materials are mainly focused on Te-based alloy, such as $Te_{93}Ge_5As_2$, with access time on the timescale of microseconds [22]. After that, a series of phase-change materials with switch speed of sub-100 ns was found, such as $Ag_4In_3Sb_{67}Te_{26}$ [23], promoting the practical application of PCM. GeTe alloy is one of the earliest phase-change materials discovered in the 1980s, which shows a Set speed of 30 ns [24] and a T_{10} of 105 °C [25]. However, the crystallization speed of GeTe will slow down sharply when the composition deviates. Therefore, the difficulty in controlling the uniformity and stability of the components inhibits the actual application of GeTe material in ePCM chips [26]. Other binary Sb_2Te_3 phase-change materials have also been extensively investigated. The crystallization temperatures are much lower than that of GeTe (<75 °C) [27]. Therefore, increasing T_c has become a major challenge for the Sb_2Te_3 alloy. Subsequently in 1987 the GeTe-Sb_2Te_3 pseudo-binary alloy phase-change

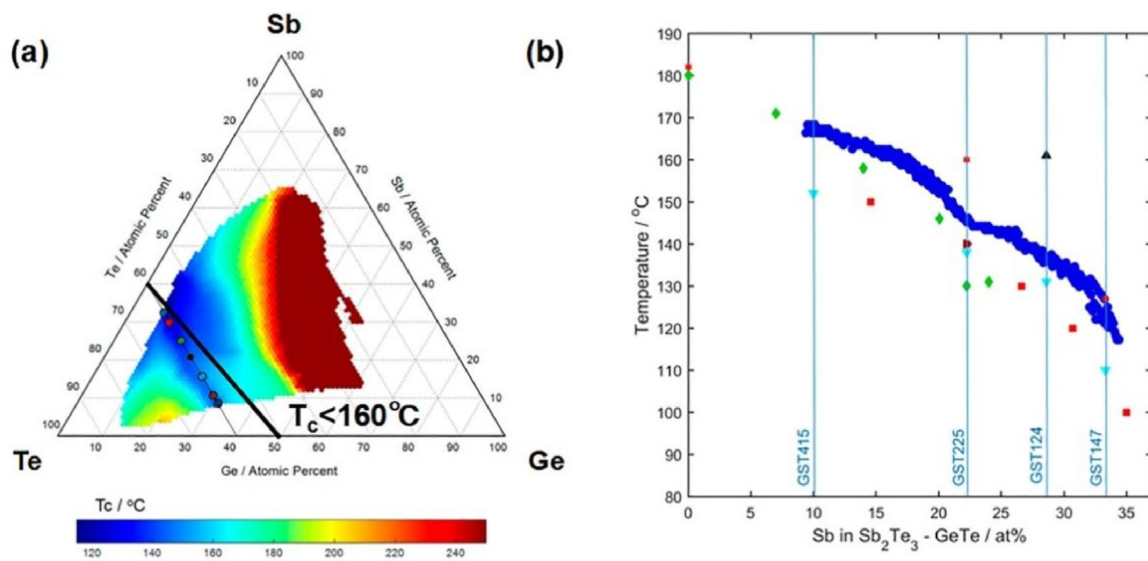

Fig. 5. Tradition Ge-Sb-Te tenary phase-change materials. (a) T_c as a function of composition in the ternary Ge-Sb-Te phase diagram. The known GeTe- Sb_2Te_3 pseudo-binary line is presented as the black line. (b) T_c along the pseudo-binary line. Copyright ©2017 American Chemical Society.

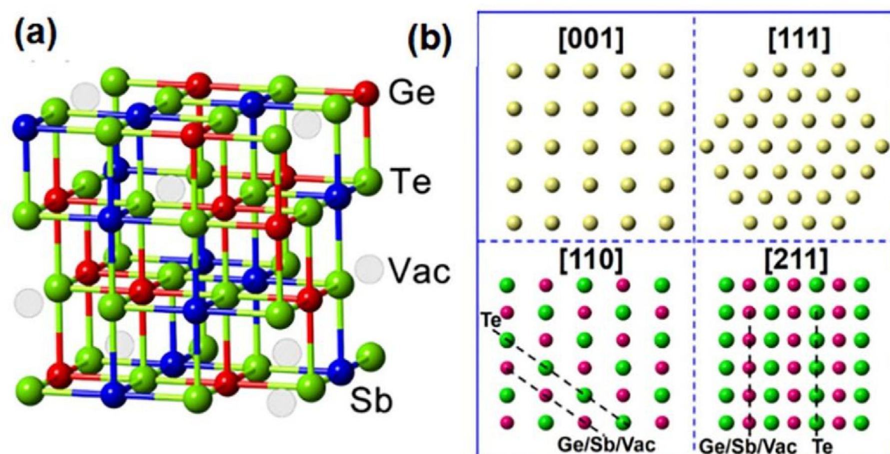

Fig. 6. Crystalline structure of $Ge_2Sb_2Te_5$ phase-change material. (a) Atomistic models of rocksalt GST, with red spheres (Ge), blue spheres (Sb), green spheres (Te), and grey circles (vacancy). (b) The atomic arrangements along the different crystallographic orientations. In the [001] and [111] views, each gold sphere is comprised of four ingredients (Te/Ge/Sb/vacancy). In the [110] and [211] views, one Set of atomic sites is taken by Te, while the other one is taken by pink spheres (Ge/Sb/vacancy). Copyright ©2016 American Chemical Society.

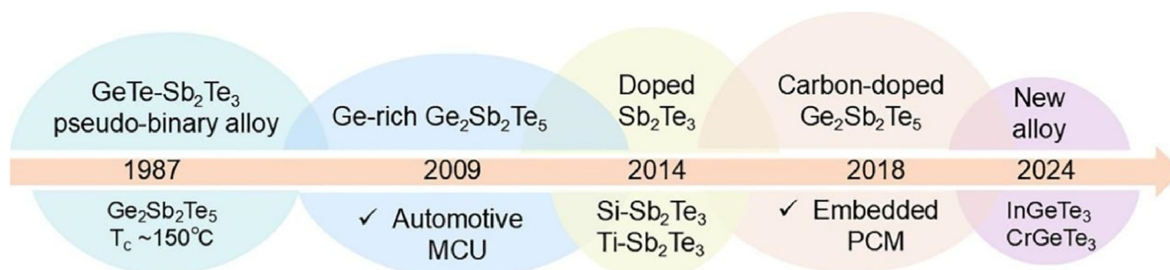

Fig. 7. Roadmap of material engineering on developing high thermal stable phase-change materials for the ePCM application.

materials with rapid phase transition process was reported by Yamada et al. [28]. Fig. 5(a) shows the Ge-Sb-Te ternary phase diagram where the pseudo-binary system $(GeTe)_x(Sb_2Te_3)_y$ is presented as the black line, showing a T_c below 160 °C [29]. In this phase-change material system, as the proportion of GeTe increases, T_c will increase accordingly, as plotted in Fig. 5(b), in which the most intensively studied phase-change material is $Ge_2Sb_2Te_5$. It shows a T_c of 150 °C and a T_{10} of 85 °C [30], which meets the temperature requirements for consumer electronics devices. In 2004, the first 4 Mb ePCM chip was successfully fabricated by using a GST phase-change material [31].

The switching mechanism of GST phase-change material has been an active field to understand the reversible rapid switching behavior. It has been reported that there is a significant amount of disorder exist in GST compounds during the rapid crystallization process from amorphous states [32]. A peculiar face-centered cubic (FCC) phase forms at about 150 °C, in which one sublattice is taken by Te, while the other sublattice is randomly occupied by 40 % Ge, 40 % Sb, and 20 % vacancy [33], as shown in Fig. 6. The FCC GST material transforms into hexagonal phase at around 350 °C [34]. Since the difference in transition resistance between the two phases after crystallization is small, the phase transition process applied to GST focuses on the transition between the amorphous and FCC phases. The metavalent bonding between metallic and covalent bonding has been considered as the fundamental bonding mechanism, which is also called the octet rule [35]. High performance phase-change material has been designed based on the mechanism of octet rule, with high speed and low power consumption [36]. However, there is still lack of the fundamental mechanism of the thermal stability and reliability of phase-change material. Hence, the research on developing ePCM will help give a deep insight into this mechanism to design high thermal stable phase-change materials.

Material engineering on developing high thermal stable phase-change materials for the ePCM has made significant progress over the past decades, as shown in Fig. 7. Since GST has shown a good performance in the phase change memory chip, early works are focusing on optimizing the composition of GST to enhance the thermal stability [37]. Ge-rich GST phase-change materials have been successfully used in the embedded memory chips in 2013 [38]. Doping method began gaining more attention to further improve the performances. Among the dopants optimized GST phase-change materials, carbon-doped GST showed a robust thermal stability with good endurance, which was used in the ePCM chips in 2018 [39]. At the same time, several studies also have been tried to improve the thermal stability of high-speed Sb_2Te_3 phase-change materials, demonstrating the high performances of Si-doped [40] and Ti-doped [41] Sb_2Te_3 phase-change materials. In addition to doping and alloying traditional PCMs with elements, a group of materials with intrinsically high thermal stability was developed recently, such as $CrGeTe_3$, $InGeTe_3$ [42]. The detailed would been discussed in this work.

3. Ge-rich GST material

3.1. Performances of Ge-rich GST

In 2009, STM presented a 90 nm 4 Mb ePCM macrocell based on GST material for the first time [43], in which a high endurance of more than one million cycles and a T_{10} of 85 °C are demonstrated. The ePCM technology has great potential to replace embedded Flash due to its low mask cost and simple process. However, the low crystallization temperature of GST material limits its further application in automotive MCUs. To improve the thermal stability of phase-change materials, extensive research has been carried out by increasing the Ge content in Ge-Sb-Te alloy, which is known as the Ge-rich GST material. It shows the advantage of no additional doping elements, and the performances of the PCM cell can be optimized by simply adjusting the composition of Ge, Sb, and Te [44–46]. In 2011, researchers proposed the Ge-rich $Ge_2Sb_1Te_2$ material with T_c of nearly 100 °C higher than the GST material [47]. In 2013, Zuliani et al. found that the increased Ge content in GST alloys

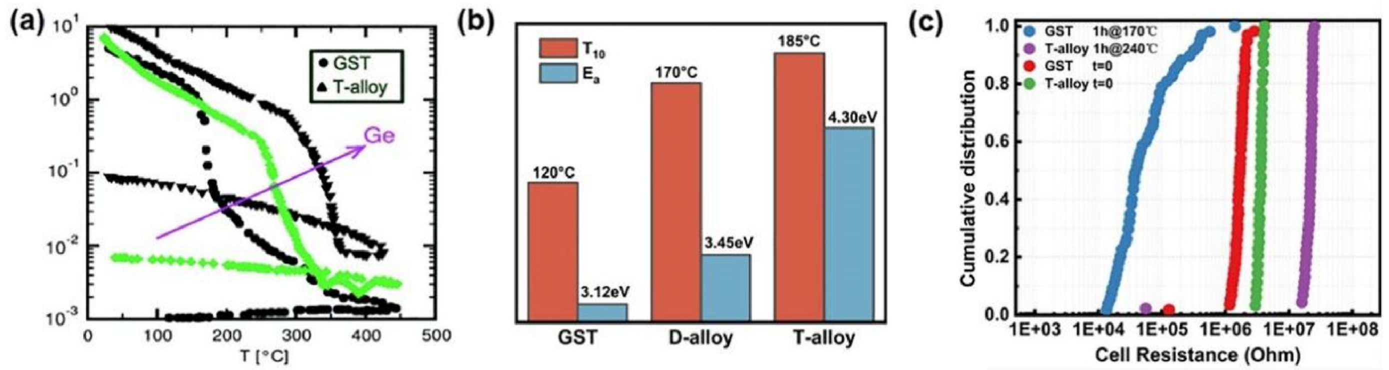

Fig. 8. Thermal stability of Ge-rich GST alloys. (a) Resistivity versus temperature curves for T-alloy compared with GST. Copyrights©2017 Elsevier Ltd. (b) Comparison of T_{10} and E_a. (c) Data retention properties for optimized T-alloy and conventional GST. Data from Ref. [133].

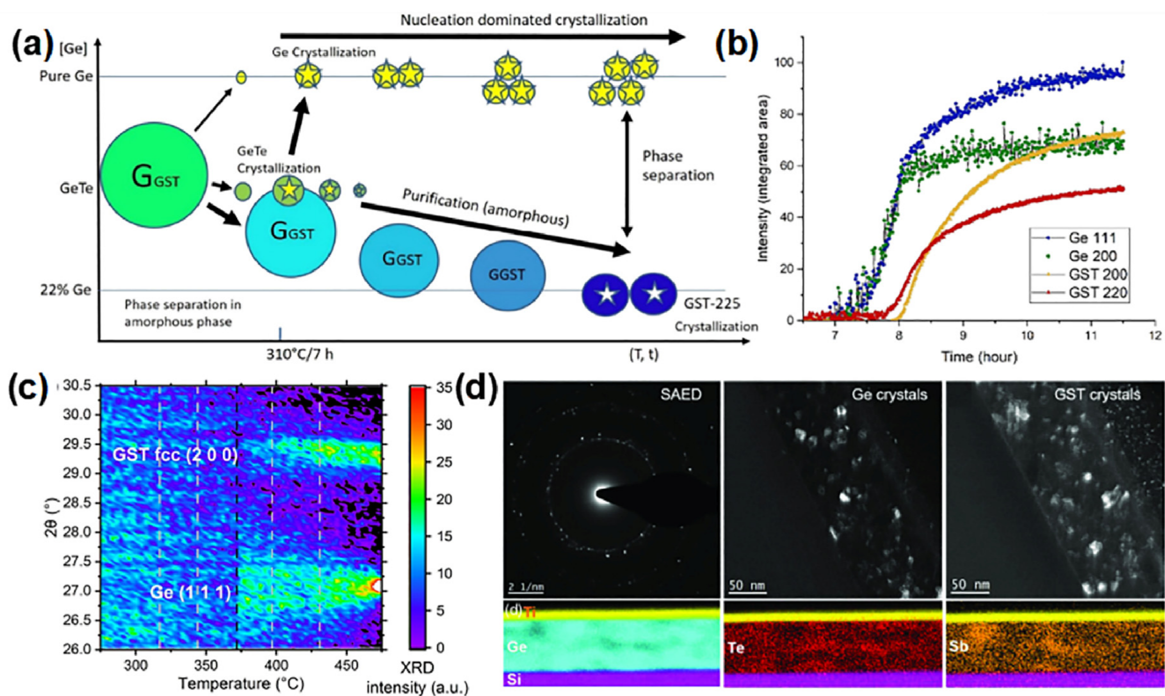

Fig. 9. Crystallization process of the Ge-rich GST alloys. (a) Evolution of the Ge-rich GST during thermal annealing. (b) Variations of two main peaks characteristic of the Ge and GST cubic phases during annealing. Copyright ©2022 American Chemical Society. (c) XRD pattern of Ge (111) and GST FCC (2 0 0) after isothermal annealing. Copyright ©2024 Springer Nature. (d) TEM images of Ge and GST crystals after annealing. Copyright ©2020 John Wiley and Sons.

enhances the thermal stability of the amorphous material [48]. Fig. 8(a) shows the resistivity as a function of temperature of Ge-rich GST and GST alloys [49], in which T_c of Ge-rich GST alloys increases with Ge content. The resistance in crystalline state is increased accordingly, which is consistent with the formation of Ge-Ge bonds [50]. The coordination number of Ge-rich GST (referred as T-alloy in Fig. 8) is close to 3.5, while in the amorphous GST film, it is 0.4. The Ge-Ge bonds, tetrahedra, and five-membered rings enhance with the Ge content in the Ge-rich GST alloys, which exist in the amorphous state and inhibit the crystallization process.

T_{10} of the Ge-rich GST material is also optimized by additional Ge content, as shown in Fig. 8(b). The optimized T-alloy of Ge-rich GST exhibits an E_a of 4.3 eV and a T_{10} of 185 °C, which is 60 °C higher than GST film. Moreover, the high thermal stability of Ge-rich GST alloys also improves the performance of PCM devices [51]. It is observed from Fig. 8(c) that the ePCM based on Ge-rich GST alloy shows a uniform Reset resistance distribution after annealing at 240 °C for 1 h, which is over 60 °C improvement compared with the PCM devices using GST alloy. The proposed PCM devices exhibit a good Reset retention soldering trail (260 °C for 40 s), and a good endurance performance up to 10^7 cycles with a resistance ratio around two orders of magnitude, indicating a great potential for the MCU data storage in automotive applications.

3.2. Mechanism of high thermal stability of Ge-rich GST alloy

Understanding the crystallization process of Ge-rich GST alloy is not only crucial for optimizing their performance in ePCM applications, but also of great significance for revealing the microscopic dynamics of the switching between different resistive states [52–54]. The crystallization process of Ge-rich GST alloy consists of four main steps [55]. Fig. 9(a) shows the evolution of the crystallization of Ge-rich GST alloys during the annealing at 310 °C: (1) During the initial stages of annealing at 310 °C, the homogeneous and amorphous Ge-rich GST alloy experiences progressive phase separation. (2) As phase separation progresses, GeTe

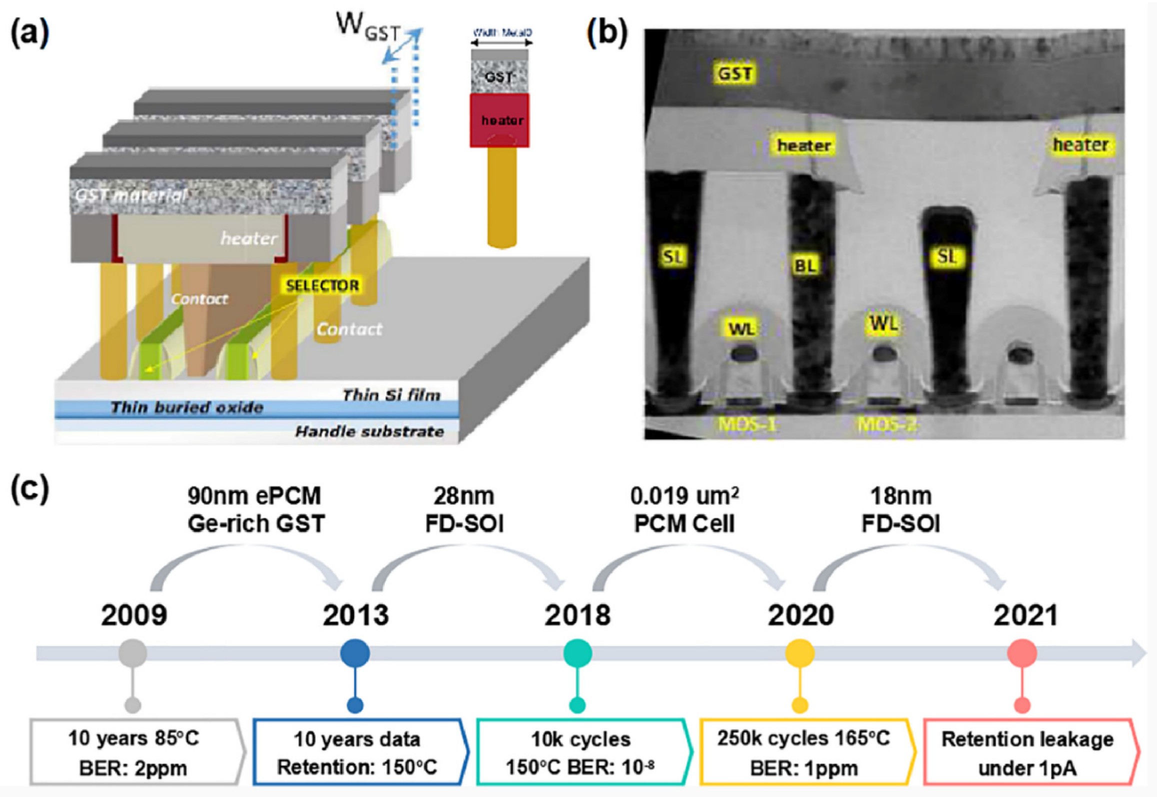

Fig. 10. The ePCM technology based on the Ge-rich GST alloys. (a) Schematic diagram and (b) cross-sectional TEM image of the ePCM cell based on the FD-SOI technology. (c) Key progress of the ePCM technology by STM focused on the Ge-rich GST alloys. Copyrights ©2022 Elsevier Ltd.

embryos are observed as the first crystallized phase. The embryonic phases act as nucleation sites, which trigger the heterogeneous crystallization of the Ge cubic phase. (3) Following the initial crystallization of GeTe embryos, the Ge phase grows by the continuous nucleation of small grains. The growth occurs as the Ge content in the remaining amorphous regions decreases, dominated by the formation of new small crystallites. (4) Once the Ge cubic phase is largely formed, the remaining amorphous regions reach the composition of GST and begin to crystallize as large grains of GST. The final step completes the crystallization process, which results in a material that contains both Ge and GST crystalline grains. Fig. 9(b) shows the variations of the integrated intensity of the two main characteristic peaks of Ge and GST phases during 310 °C annealing. The result confirms the earlier formation of Ge phase prior to GST phase. The intensity of the Ge peaks reaches 80 % of the final value within the first 30 min before the nucleation of GST phase. Compared to Ge, the GST phase builds up more slowly and the GST peaks begin to increase approximately 20 min after the Ge peaks have almost reached their maxima, indicating the existance of both Ge and GST crystalline phases in the Ge-rich GST alloys.

Remondina et al. [56] demonstrated the crystallization process of Ge-rich GST alloy through thermal annealing at various temperatures. Fig. 9(c) shows the XRD pattern of Ge (111) peak and GST (200) peak after annealing. After annealing at 310 °C, the sample presents phase separation in the amorphous domain. When the temperature is increased to 337 °C, a broad and weak peak corresponding to the Ge (111) peak appears in the XRD pattern, indicating the crystallization of Ge. As the annealing temperature continues to increase, both Ge (111) and GST (200) peaks emerge in the XRD pattern, indicating that GST has also crystallized. Moreover, Luong et al. [57] observed the coexistence of Ge and GST grains after annealing at 400 °C for 30 min through transmission electron microscopy (TEM) analysis, as shown in Fig. 9(d). The larger crystalline regions are the GST alloy, while the smaller grains are cubic Ge phases.

3.3. The ePCM chip based on Ge-rich GST material

STM has been dedicated to the ePCM technology in the field of automotive MCU for a long time [58–60]. In 2018 Aranud et al. proposed a 28 nm FDSOI ePCM solution based on the Ge-rich GST material [61], offering a new eNVM solution for automotive MCU applications. Fig. 10 shows the co-integration scheme of PCM and CMOS technology based on FDSOI substrate [62]. This technology demonstrated a 5 V transistor with high analog performance. The PCM cells maintained a programming window of two orders of magnitude after one million cycles. The PCM cells exhibited a low bit error rate (down to 10^{-8}) after multiple bakes at 150 °C and 10^4 operation cycles, which is compatible with the stringent requirements of the automotive industry.

Furthermore, Aranud et al. [63] enhanced the 28 nm FDSOI-PCM solution in 2020 using a bipolar junction transistor selector, integrating triple gate oxide devices with an cell size of 0.019 μm^2. The PCM array is based on the Ge-rich GST alloy organized with isolating bit and word line. The innovation not only increased storage density but also demonstrated exceptional reliability, meeting the automotive grade-0 reliability criteria, with a wide reading window obtained even after 2.5×10^5 write operations at 165 °C. Furthermore, to emulate the thermal stress of reflow soldering, the 16 MB PCM array was kept at 265 °C for 210 s. It reaches the target of Reset retention for automotive applications, ensuring data integrity and performance under extreme conditions. In 2021, Ge-rich GST-based PCM was successfully integrated into the 18 nm FDSOI process by STM [64]. The advanced technology node offers better performance and lower power consumption, representing the most advanced eNVM MCU solution so far [65].

3.4. Challenge and prospects

Although Ge-rich GST alloy shows the advantage of high thermal stability and good data retention, it also has significant drawbacks that

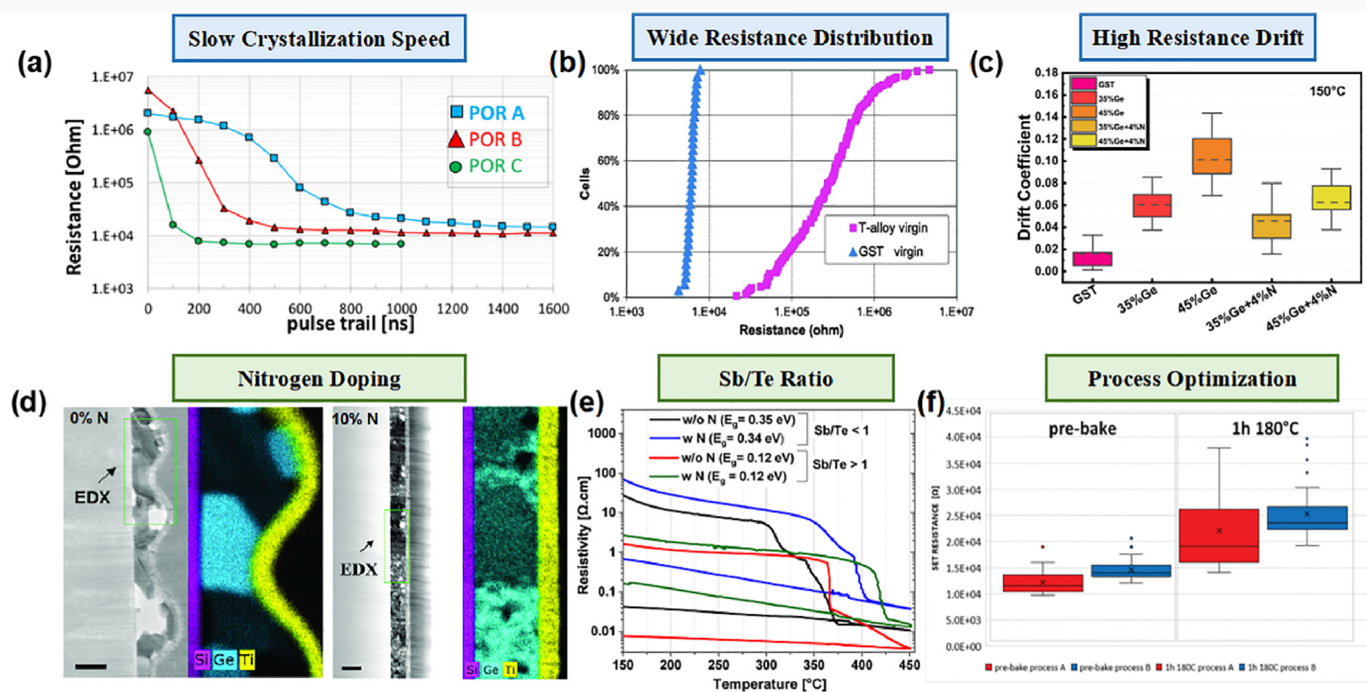

Fig. 11. Drawbacks of Ge-rich GST alloys and improvement methods. (a) Crystallization speed of GST and Ge-rich GST. (b) Virgin cells resistance distribution processed with GST and Ge-rich GST. Copyrights ©2017 Elsevier Ltd. (c) Drift coefficient for the LRS at 150 °C measured for different materials. (d) TEM images and EDX maps of Ge-rich GST without and with N. Copyright ©2020 John Wiley and Sons. (e) Resistivity versus temperature curves for Ge-rich GST alloys with Sb/Te $<$ 1 and Sb/Te $>$ 1, without and with N. Copyright ©2024 AIP Publishing. (f) Data retention properties for two different processes after 180 °C baking.

cannot be overlooked. The first drawback of Ge-rich GST alloy is the slow crystallization speed, as shown in Fig. 11(a). POR C refers to conventional GST, while POR B represents Ge-rich GST. It is observed that Ge-rich GST is three times slower than conventional GST [48]. The slow Set speed of Ge-rich GST can be explained through its crystallization mechanism. The Ge-rich GST alloy undergoes a phase separation process before crystallization, delaying the start of crystallization. The crystallization process of Ge-rich GST alloy involves the growth of two different grains, Ge and GST, thus increasing the overall time for crystallization [66]. POR A in Fig. 11(a) represents Ge-rich GST deposited through process optimization. It exhibits an enhanced crystallization speed, which locally modifies the material composition in the melted region, effectively mitigating the segregation of Ge. The second drawback is the higher Set resistance and wider initial resistance distribution after the process [67], as shown in Fig. 11(b), which is due to the segregation of Ge during the high temperature process. The third drawback is the higher resistance drift, as shown in Fig. 11(c), where the Set resistance drift of Ge-rich GST at 150 °C is higher than that of GST [68]. Laurin et al. demonstrated that the high Set resistance drift is caused by the element segregation and amorphous residuals during its crystallization process. For the first time, the amorphous residuals were observed in the activation area of the PCM devices using STEM [69].

Many efforts have been made to address these challenges. Navarro et al. [68] proved that nitrogen doping can effectively enhance the resistance stability. As shown in Fig. 11(c), the doped nitrogen forms strong Ge-N bonds with germanium, reducing the diffusivity of Ge and thereby decreasing the resistance drift over time. Moreover, Fig. 11(c) displays the XRD patterns of N-doped Ge-rich GST alloys after annealing from 340 °C to 500 °C, demonstrating that the incorporation of N inhibits the transformation to hexagonal GST phase and increases crystallization temperature [70]. The TEM images performed on the films with and without N are shown in Fig. 11(d), revealing that the undoped layer is characterized by larger grain sizes with a higher propensity for void formation. The increasing of N content shows a finer morphology made of smaller crystalline grains, thus enhancing the device functional yield after fabrication process. Daoudi et al. [71] demonstrated a faster crystallization speed by adjusting the Sb/Te ratio, as shown in Fig. 11(e), while retaining the advantages of high crystallization temperature. Palumbo et al. [72] successfully mitigated Ge segregation after process through carbon implantation into Ge-rich GST alloys. No open bits were observed after 10^5 cycles at 150 °C, exhibiting enhanced device reliability and improved data retention at high temperature. Furthermore, the process optimization not only significantly enhances the crystallization speed of Ge-rich GST alloy but also improves its data retention properties, as illustrated in Fig. 11(f). The Ge-rich GST cells fabricated using the optimized process demonstrate a uniform resistance distribution even after annealing at 180 °C for 1 h, which can be attributed to the reduction in Ge segregation through process optimization.

In conclusion, while significant achievements have been made, the Ge-rich GST alloys still face critical challenges for high performance ePCM. Substantial research efforts are required to overcome these limitations through comprehensive optimization of material property, device design, and fabrication process. This will make Ge-rich GST alloys more suitable for advanced ePCM technologies that demand high thermal stability and reliability [73,74].

4. Carbon doped GST material

4.1. Light element doped GST

Doping has been proved to be one of the most effective strategies to enhance the properties of GST phase-change materials. Both experimental studies and theoretical calculations have demonstrated that among several dopants, such as Si [75–77], O, N, and Ta [78], C is particularly effective in improving the thermal stability and endurance of GST materials. Nitrogen-doped GST (NGST) material can be prepared through reactive sputtering or ion implantation. Previous studies have demonstrated that nitrogen doping in GST films significantly enhances

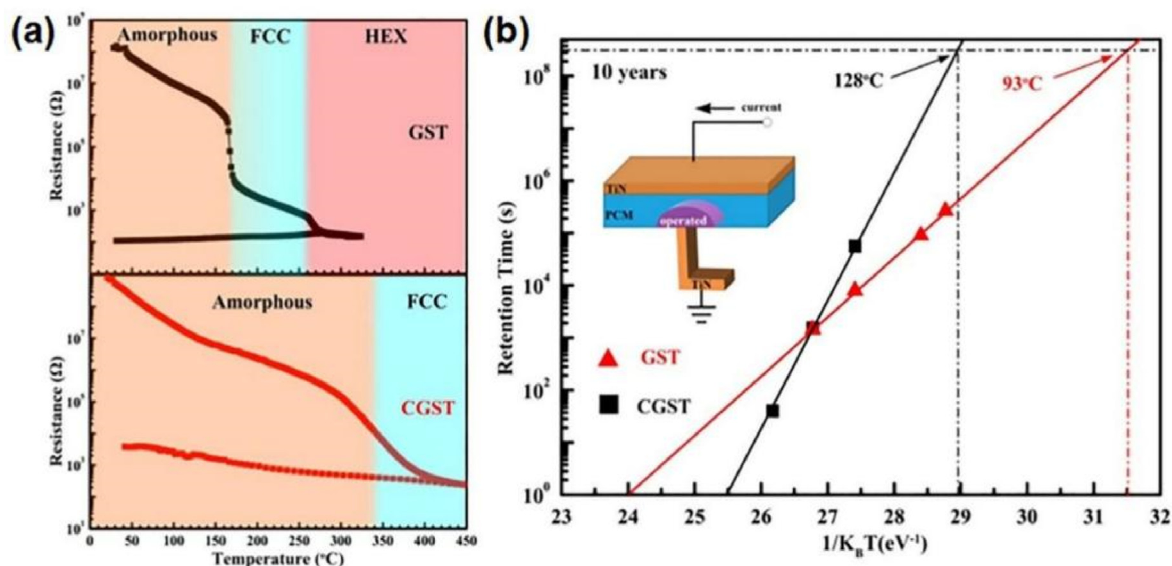

Fig. 12. Temperature dependence of the sheet resistance and corresponding data retention characteristic. (a) Sheet resistances as a function of temperature for GST and CGST materials. (b) Arrhenius extrapolation plots of failure time versus $1/k_BT$ for the GST and CGST-based PCM devices. The inset is the schematic diagram of PCRAM cell structure with the blade TiN electrode. Copyright ©2020, American Chemical Society.

the stability of the amorphous state, increasing the crystallization temperature of GST [79–81]. Nitrogen atoms tend to form Ge-N clusters with Ge, distorting the structure of neighboring atoms [82]. This distortion impedes the crystallization process and slows the speed of grain growth. NGST-based PCM cell exhibits excellent performance in terms of power consumption, durability, and the potential for multi-bit data storage [83, 84]. Oxygen is also an attractive dopant for GST. The preparation of oxygen-doped GST (OGST) material follows a similar deposition process to NGST. Studies indicate that the dissociation energy of O is low, resulting in a low formation energy for OGST [85,86]. Oxygen doping introduces additional nucleation sites, leading to faster phase transitions in OGST. However, high oxygen content in GST films will result in formation of a germanium-deficient hexagonal phase (e.g., $GeSb_2Te_4$ or Sb_2Te_3) upon annealing, resulting in a severe resistance drop at low temperatures and thus affecting the electrical properties of PCM devices [87].

In 2011, Yong et al. [88] studied the effect of carbon doping on the structure and electronic properties of amorphous CGST (a-CGST) using *ab initio* molecular dynamics simulation. The calculations show that carbon dopants fundamentally change the local order of the amorphous network by significantly increasing the number of tetrahedral Ge atoms compared to Si, N, and O dopants. ABAB square rings in amorphous phase-change materials can be used as nucleation sites of crystals. The density of ABAB rings in amorphous CGST is much lower than those of undoped amorphous GST, NGST, and OGST, which implies the outstanding stability of amorphous CGST. Therefore, carbon doping has been widely discussed and studied in these years.

4.2. Switching performance of CGST

The research has proved that carbon dopants are very effective in extending the covalent properties and enhancing the stability of amorphous GST (a-GST) by molecular dynamics simulations [82–84]. Borisenko et al. [92] found that in a-CGST C atoms were inclined to form C-Ge bonds and C-C bonds, indicating that the germanium carbide phase and atomic scale carbon clusters appeared inside the material structure. The main structure of a-CGST is the distorted squares and square fragments of Ge(Sb)-Te-Sb(Ge)-Te atoms, similar to the elementary building blocks of the corresponding crystalline structures of the metastable FCC phase of pure GST.

An outstanding advantage of CGST phase-change materials is the simplicity in preparation as well as the ability to easily incorporate carbon atoms from both the precursor and co-reactant materials. In many studies, CGST thin films have been prepared using the magnetron sputtering tool, with co-sputtering of elemental carbon and GST alloy target. Extensive experimental evidence has demonstrated that the incorporation of carbon atoms into GST can substantially enhance the thermal stability of the material, particularly by increasing both the T_c and T_{10} [93,94]. For instance, the study by Cheng et al. [95] shown in Fig. 12(a) reveals that the resistance values of CGST in both amorphous and crystalline states are higher than that of undoped GST, suggesting that carbon doping alters the electronic characteristics of the material. Furthermore, CGST exhibits a significantly higher T_c compared to GST. The phase transition from FCC to hexagonal structure is effectively suppressed, thereby stabilizing the metastable phase. The fitting curve of data retention in Fig. 12(b) indicates that the T_{10} for CGST is elevated to 128 °C, which is 35 °C higher than GST, demonstrating an improvement in the data retention capability of the material. Moreover, the properties of CGST can be further optimized by adjusting the carbon doping concentration. Zhou et al. [96] for the first time demonstrated experimentally that by fine-tuning the carbon doping level, the T_c of CGST can be increased to 238 °C, while the T_{10} can be enhanced to 145 °C, indicating a significant improvement in thermal stability.

PCM devices based on CGST exhibit superior electrical performance compared to those undoped GST. The CGST PCM cells show increasing resistance values in both low-resistance state (LRS) and high-resistance state (HRS), a significant reduction in the Reset operation voltage, and enhanced cycling endurance [90–92]. Thermoelectric simulations indicate that the CGST phase-change material, with its higher resistivity and lower thermal conductivity, effectively minimizes heat dissipation during the Reset process [97–100]. This reduction in heat dissipation leads to a decrease in overall power consumption. However, it is important to note that excessive carbon content presents detrimental effects on the switching performance of CGST-based devices [101]. High level of carbon doping lead to a slowed Set operation speed and a reduction in the ON/OFF ratio, which negatively impacts the device's switching characteristics and operational efficiency [102]. Based on the above conclusions, the high thermal stability and excellent cycle endurance of CGST ensure its suitability for ePCM chips.

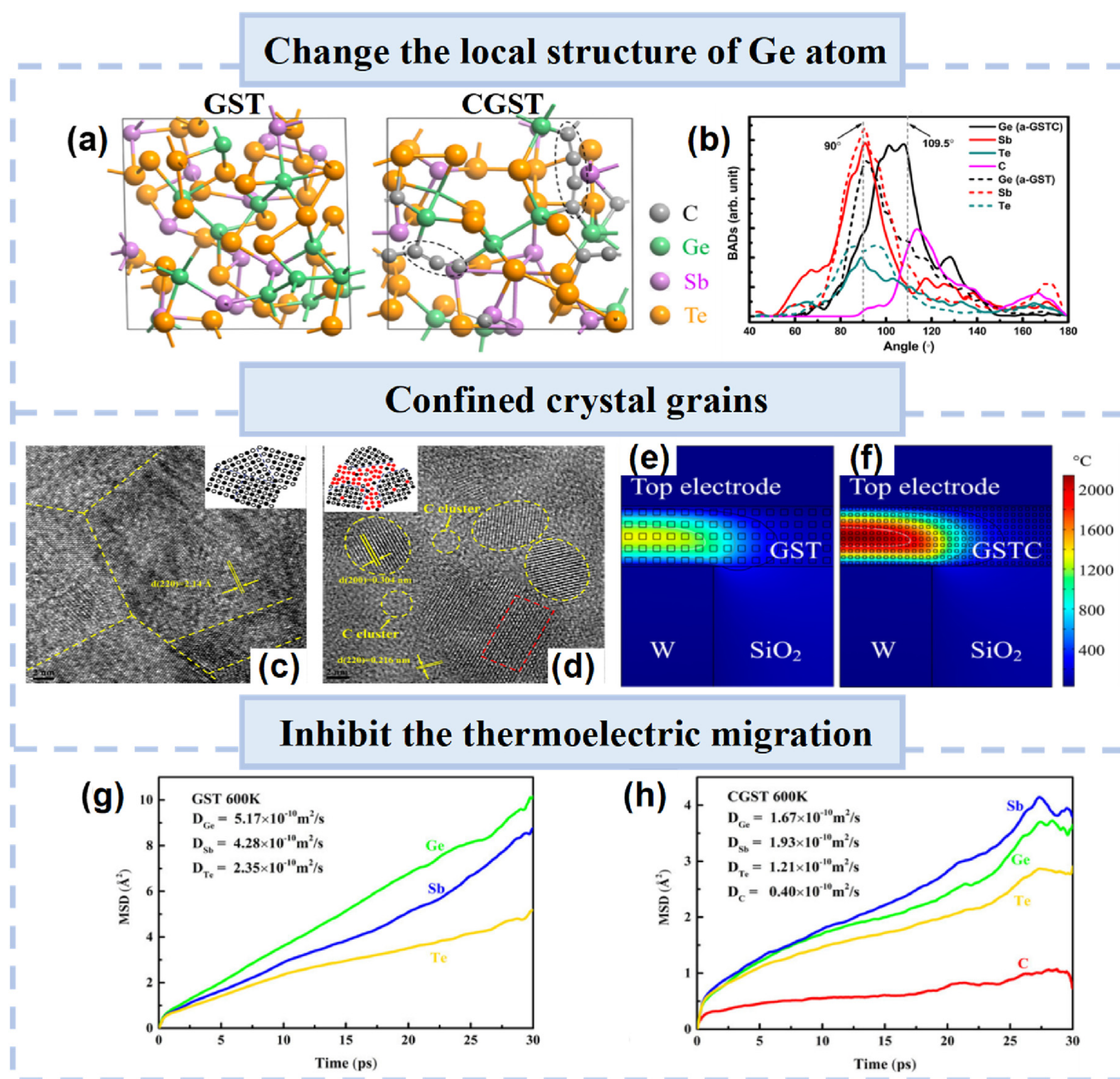

Fig. 13. Mechanism of enhanced thermal stability by carbon doping. (a) Amorphous structures of GST and CGST at 300 K. (b) The BAD around the atoms. The vertical dash lines indicate the octahedral (90°) and tetrahedral (109.5°) angles, respectively. HRTEM images of (c) FCC GST and (d) FCC CGST film, and schematic illustrations of corresponding crystalline phases in the insets. Simulated RESET temperature distributions in PCM cells with different grain sizes of (e) GST and (f) CGST layers. Copyright ©2014, American Chemical Society. MSD curves and diffusion coefficient of each atom in (g) GST and (h) CGST at 600 K. Copyright ©2019, American Chemical Society.

4.3. *Mechanism of enhanced thermal stability of CGST material*

Researchers have conducted extensive studies on the phase change mechanisms of CGST materials, focusing particularly on how carbon doping enhances the thermal stability and durability of phase-change materials through a combination of experiment and calculation.

The doped carbon atoms change the local structure of Ge atom significantly. The calculation results demonstrate that C atoms exert a significant influence on the atomic and electronic structure of a-GST, with an increase in tetrahedral Ge coordination significantly enhancing the amorphous stability of PCM [88,89,91,102]. Fig. 13(a) shows the amorphous structure of GST and CGST. Fig. 13(b) gives the corresponding calculations results of bond angle distribution (BAD). The peak position in the Ge-centered BAD significantly shifts to larger angle toward the tetrahedral angle (109.5°) in a-CGST, indicating larger portion of tetrahedral Ge sites with C addition [97]. The reconstructed 3D mapping by atomic probe tomography (APT) of a-CGST material reveals that the concentrations of C and Ge change almost synchronously. While the Sb and Te concentrations are significantly reduced in the C/Ge-rich regions, suggesting a preferential bonding interaction between C and Ge atoms in a-CGST [100]. EXAFS data further indicates that carbon atoms partially substitute Ge and Te in Ge-Ge and Ge-Te bonds, resulting in the formation of Ge-C bonds. The sp^3 hybridization between Ge and C contributes to the network rigidity by reducing ABAB ring motifs, thereby improving the thermal stability of the system [103]. Raman spectrum also demonstrated the reduction of tetrahedral units $GeTe_{4-n}Ge_n$ ($n = 1, 2$) induced by carbon doping [103]. However, the incorporation of tetrahedral Ge atoms reaches saturation at carbon doping concentrations between 5 and 10 at.%, after which the tetrahedral Ge bonding begins to decrease [102].

Carbon atoms are beneficial to form three-dimensional confined structures. The microstructural characteristics of GST and CGST can be directly observed using TEM analysis [97,103,104]. The TEM images of CGST, along with Fast Fourier Transform (FFT) diffraction rings, display weak intensity. It suggests that the crystallization process in CGST is significantly suppressed. High-resolution TEM (HRTEM) images shown in Fig. 12(c) and (d) presented by Zhou et al. [97] exhibit the crystallization behavior of GST and CGST after annealing at 250 °C and 400 °C,

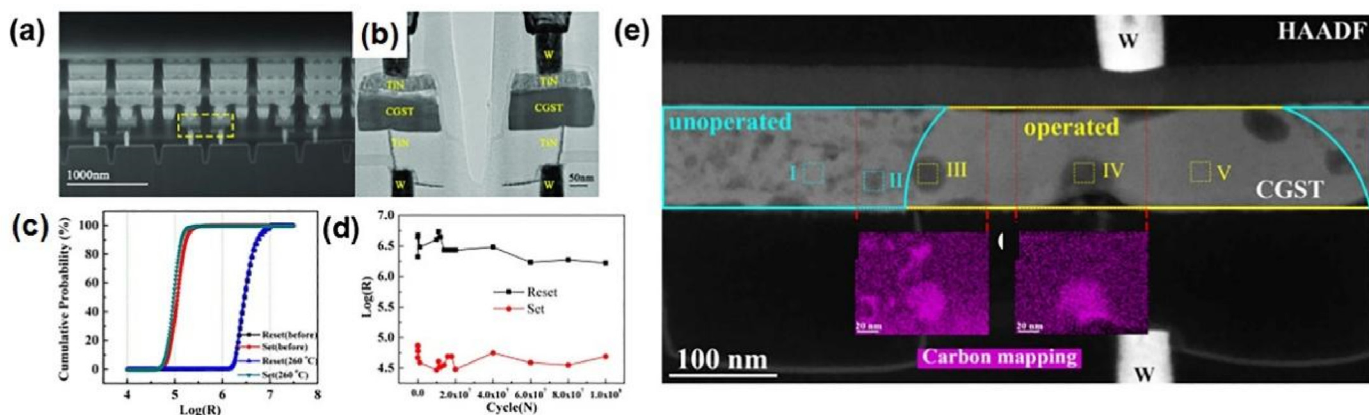

Fig. 14. The ePCM chips based on carbon-doped GST phase-change materials. (a) TEM cross-sectional image of the PCM chip. (b) TEM image of the PCM cells. Copyright ©2019 WILEY-VCH Verlag GmbH & Co. KGaA, Weinheim. (c) Reset and Set distribution (16 Kb cells) before and after the soldering test at 260 °C for 5 min. (d) Typical cell cyclability of the CGST-based PCM 128 Mb chip. Copyright ©2018, IEEE. (e) The cross-sectional STEM-HAADF image of a failed CGST PCM cell and C mappings of the CGST film obtained from the red dotted rectangles. Copyright ©2020, American Chemical Society.

respectively. Most of the C atoms in CGST films are randomly distributed in amorphous clusters that surround the crystal nuclei which effectively limits the grain growth in three dimensions. A portion of the C atoms is incorporated within the grains, where they either substitute for Te atoms or occupy the interstitial sites. Three-dimensional APT reconstructions of crystalline CGST (c-CGST) reveal carbon-rich clusters with dimensions of approximately $4 \times 5 \times 10$ nm^3. Notably, the distribution of Ge, Sb, and Te within the regions is significantly diminished, which further supports the notion that C atoms predominantly localize around the GST grains [100]. The 3D confinement effect of C atoms contributes to a reduction in the grain size of the FCC phase. According to previous research, the grain size of GST after in-situ electric field operation ranges from 100 to 140 nm [105], whereas the grain size of CGST after electrical pulse operation failure is only between 20 and 50 nm [106]. Fig. 13(e) and (f) show the electrothermal simulation results of heat distribution in the Reset programming of GST and CGST PCM devices based on different grain sizes [97]. The peak temperature in the CGST layer is significantly higher than that of the GST layer. This suggests that the smaller grain sizes in CGST inhibit heat dissipation, which enhances thermal stability and lowers the Reset current of PCM devices.

Carbon atoms inhibit the migration of GST atoms. The crystal growth rate at the amorphous-crystal interface near carbon atoms is significantly reduced, particularly near the carbon-rich clusters. This reduction in growth rate is attributed to the presence of carbon, which contributes to the reduced operation speed of CGST phase-change memory devices. Fig. 13(g) and (h) present the mean square displacement (MSD) and diffusion coefficients (D) of the atoms in both GST and CGST at an ambient temperature of 600 K. The presence of non-diffusive C clusters in CGST inhibits the long-range thermal- and electro-migration of Ge, Sb, and Te atoms [100]. This inhibition is a key factor in the enhanced endurance of CGST PCM cells, as it suppresses the atomic migration and stabilizes the material over prolonged cycling.

4.4. The ePCM chip based on CGST material

After extensive research and developments, CGST phase-change materials have reached an increased level of maturity. Researchers in shanghai institute of microsystem and information technology (SIMIT) have successfully fabricated highly reliable ePCM chip based on the CGST material at 40 nm node. The capacity of the chip is 128 Mb with a chip yield of 93.3 % [107]. Fig. 14(a) presents a cross-sectional TEM image of the chip array, while Fig. 14(b) shows the TEM image of two independent PCM cells [108]. The chip employs a TiN L-type electrode as the heater. The ePCM chip is operated with current pulses down to 20 ns with an on/off ratio larger than two orders of magnitude and T_{10} of 128 °C. Fig. 14(b) shows the distribution of Reset and Set resistance values before and after the soldering test at 260 °C. After a 5 min baking process, a clearly detectable resistance window remains, demonstrating the good stability of the devices. Fig. 14(d) shows that the device can perform more than 10^8 switching cycles, implying its suitability for applications demanding both high thermal stability and exceptional cycle durability [107]. Furthermore, Liu et al. [109] developed a stepped programming and validation method to demonstrate multilevel storage (MLC) functionality of CGST alloy. The read endurance at 0.3 V is up to 10^9 cycles, confirming the excellent performance of the CGST-based PCM in terms of read endurance. These results prove the great potential of CGST-based ePCM chips for high-reliability multilevel storage applications.

To investigate the impact of C atoms on the electrical performance of PCM devices, Cheng et al. [110] performed a failure analysis on CGST based PCM chips. The cross-sectional TEM image of the device is presented in Fig. 14(e), clearly showing the operated active region and the unoperated region. The purple signal at the bottom corresponds to the EDS analysis of the C element, which reveals that C atoms accumulate in the dark contrast regions. The gradual segregation and aggregation of the C element contribute to a decrease in the Reset resistance value during cycle operation. The C atoms migrate toward the active region under current pulses, inhibiting grain growth and improving reliability. The redistribution of C dopants is crucial for optimizing PCM performance and offers insights into C-doped material systems.

CGST has emerged as one of the most promising materials for ePCM applications, showing good thermal stability, reliability, and cycling durability. Although CGST devices have slower Set speeds, it is appropriate for embedded data storage applications that prioritize long-term stability and energy efficiency. Additionally, enhancing the uniformity and consistency of CGST at the microscopic level is essential. This can be accomplished by optimizing the deposition process of phase-change material film. The practical application of CGST-based PCM can be enhanced by optimizing the device structure and circuit design, which will improve the efficiency and reliability of CGST-based PCM chips.

5. Optimization of Sb_2Te_3 based material

As mentioned above, GST as a representative of chalcogenide materials, is the most widely studied alloy. Although GST-based phase-change memory shows good performance, there are still many works needed to be performed. Compared to GST, Sb_2Te_3 has a lower T_m and higher operation speed, which has also attracted a great deal of attention in the past decades. However, the much lower T_c of Sb_2Te_3 leads to an unstable amorphous phase and poor data retention. Therefore, increasing the thermal stability is a major challenge for applications of Sb_2Te_3-based

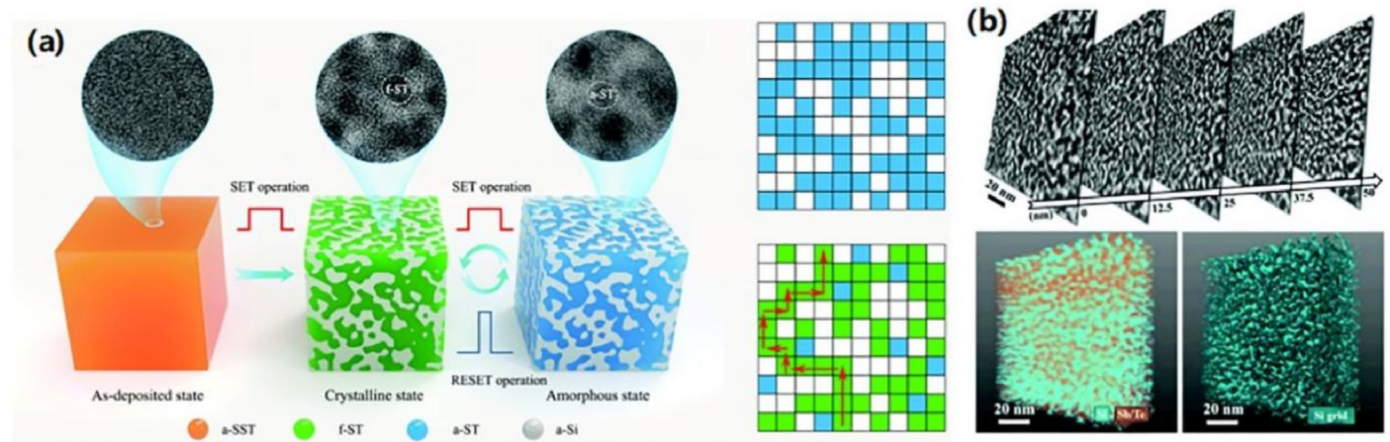

Fig. 15. The structural, thermal and electrical characteristics of SiSbTe. (a) Schematic diagram of reversible phase-transition processes in bicontinuous structure. (b) Tomographic reconstruction insights into the 3D bicontinuous structure of crystallized SiSbTe material.

PCMs. Reducing the film thickness of Sb_2Te_3 to the sub-nanometer scale has been reported to be an effective way to increase T_c, showing a T_c of 75 °C at 1 nm thick and 200 °C at 0.75 nm thick [111]. However, the thickness of the film prepared by laboratory-grade equipment is often more than 2 nm. For this purpose, a variety of dopants are introduced into Sb_2Te_3 to improve its thermal stability. Based on the successful cases of doping light elements into GST material, many studies have also introduced light elements C [111–115], N [116,117], and O [118,119] into Sb_2Te_3 materials. The doping of light elements effectively improves the thermal stability and the resistance of as deposition Sb_2Te_3 film. However, the light elements dopants with small atomic radius are distributed in the lattice gap or interface, which are capable of forming enrichment and limiting the growth of grains, reducing the crystallization speed of Sb_2Te_3. However, excessive light element doping would sacrifice the electrical properties of PCM and lead to phase separation which reduces the reliability of PCM.

In addition to the above-mentioned doping elements, the Si-doped Sb_2Te_3 (SST) [120–124] phase-change material is widely used in ePCM. The phase transition mechanism is different from that of GST. In 2021, cheng et al. [125] combining the advanced 3D tomography techniques and TEM presented that the crystalline SST films have a uniform equiaxial structure in 3D space, which is composed of reversible Sb_2Te_3 and amorphous Si phases, well nesting with each other. Fig. 15(a) illustrates the phase transition mechanism of SST materials. The as-deposited SST film presents a homogeneous amorphous state with high resistance. After Set operation, a specific bicontinuous structure is formed, i.e., the amorphous Si region and the nanocrystalline Sb_2Te_3 region are nested to form a low resistance state. When Reset it again, the nanocrystalline Sb_2Te_3 returns to the amorphous state, and the amorphous Si region and the nanocrystalline Sb_2Te_3 are nested to form a high resistance state. A general percolation model is used to explain the relationship between the electrical properties and microstructure. Theoretically, when the site occupancy probability is 30 %, half of the Sb_2Te_3 region can crystallize to form a complete conductive pathway. Fig. 15(b) shows five HAADF-STEM slices along the thickness direction and a visualized 3D tissue structure of the reconstructed. The tissue structure of the evenly distributed slices shows that the Si region and the Sb_2Te_3 region were homogeneously mixed.

In 2011, Li et al. [126] used the first-principles AIMD calculation to confirm that the formation energy of SST alloy was higher than that of the separated Si and Sb_2Te_3 phases, indicating that SST was easier to form phase split. In 2014, Wang et al. [127] used a first-principles-based molecular dynamics simulation method to simulate the bonding behavior of the interface between amorphous Si and amorphous Sb_2Te_3 materials at the nanoscale, and found that: (1) Through the spatial effect of the atomic "channels" of the amorphous interface, the arrangement of the Te network is significantly distorted and separated from the p-orbital bond angle in conventional phase-change materials. (2) Through the electronic "channels" of the amorphous interface, highly localized electrons in the form of lone pairs are "projected" from the amorphous Si to Sb_2Te_3 by proximity effects. From the perspective of bonding and electron distribution, the intrinsic mechanism of Si doping to improve the thermal stability of Sb_2Te_3 is explained in more detail. It is worth mentioning that the metastable FCC Sb_2Te_3 phase can be remarkably preserved even

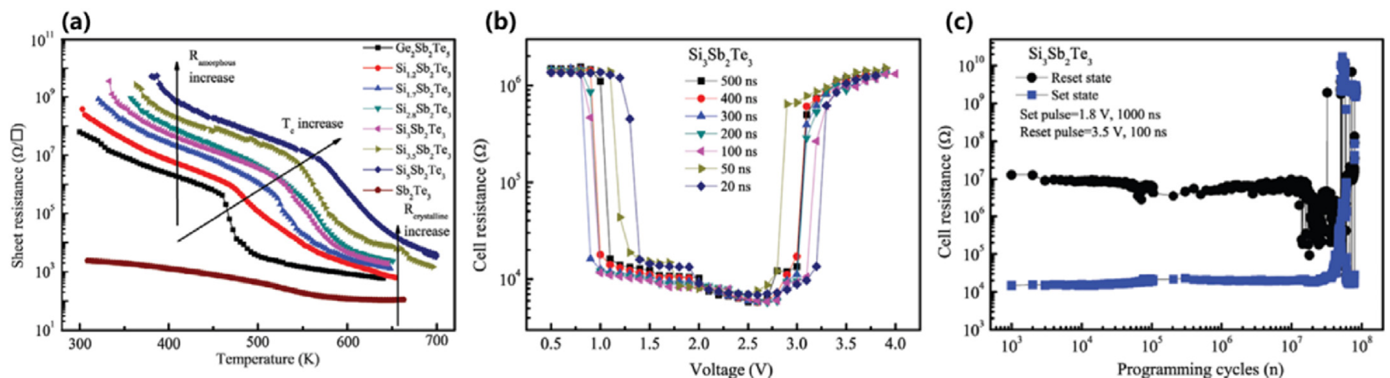

Fig. 16. Switching performances of $Si_xSb_2Te_3$ films and devices. (a) Temperature dependence of the sheet resistance R_s of the Sb_2Te_3, GST, and $Si_xSb_2Te_3$ films. (b) Resistance-voltage characteristics of PCM cell based on $Si_3Sb_2Te_3$ material for different voltage pulse widths. (c) Endurance characteristics of PCM cells based on $Si_3Sb_2Te_3$ material. Copyright ©2011, IOP Publishing, Ltd.

Table 1
Performance of the SST-based and GST-based PCM devices [128].

	Reset current (μA)	Set speed (ns)	Drift coefficient at HRS/LRS at 65 °C	Drift retention at 85 °C	Endurance
SST	550	100–820	0.01/0.01	48 h	$<10^7$
GST	650	60–100	0.1/0.065	25 min	$<10^5$

above 370 °C in this bicontinuous system. Considering the excellent thermal stability of SST material, it is a potential candidate for ePCM, especially in automotive electronics applications. As the Si doping concentration increases, both the T_c and E_a increase. The SST material exhibits a higher T_c and binding energy (E_a) compared to GST [123].

Fig. 16(a) shows the sheet resistance of $Si_xSb_2Te_3$ and GST films as a function of temperature, with a heating rate of 13 C/min. With the increase of Si content, the T_c of SST increases, and the resistance of amorphous state also increases. Although the Si doping concentration can improve the thermal stability of Sb_2Te_3 materials, the excessive Si atoms will also lead to an increased operation speed and energy cost, so it is necessary to select an appropriate doping concentration. Fig. 16(b) shows the Set and Reset operations of $Si_3Sb_2Te_3$-based PCM cell driven by different voltage pulse widths. From the data in Table 1, the T_{10} of $Si_3Sb_2Te_3$ reached 120 °C, which was significantly improved compared with GST. Fig. 16(c) shows the endurance characteristic of $Si_3Sb_2Te_3$ with 10^7 endurance switching cycles.

In 2024, IBM [128] presented the performance of SST-based PCM chip, exhibiting significant advantages over GST chips, as shown in Table 1, particularly in terms of data retention capability at 85 °C, which is more suitable for the requirements of eNVM applications. Although SST has good thermal stability, its slow read/write speed limits its further applications. Introducing another doping element is proposed to solve this issue.

Afterwards, the octahedral "gene" principle is proposed by Song et al. [129], that is, when performing doping modification, the selected dopant atoms, upon incorporation into the matrix material, can form stable chemical bonds with the atoms in the matrix. These bonds then enable the formation of local octahedral or octahedral-like structures. Due to the abundance of stable local octahedral configurations in the amorphous state, the time required for nucleation is shortened during the phase transition to the FCC structure, thereby enhancing the crystallization rate.

Based on this principle, Zhu et al. successfully synthesized Ti-Sb_2Te_3 (TST) phase-change material by introducing titanium into Sb_2Te_3 in 2014 [41]. This material demonstrated remarkable performance, with a phase-change speed of 6 ns, a cycling endurance of 10^7 cycles, and power consumption values that are superior to those of GST. Fig. 17(a) depicts the atomic configuration of amorphous TST, as derived through melt-quenched molecular dynamics simulations. Meanwhile, Fig. 17(b) and (c) provide a comparative analysis of the coordination number (CN) and BAD between the amorphous TST and GST material. The computational results indicate that Ti elements tend to have a coordination number of 6 or 7 in TST, with a peak bond angle of approximately 85°, which is very close to the ideal rock-salt structure. Considering the coordination numbers and bond angle distributions of Sb and Te elements, we deduce that the Ti-centered atomic motifs (TCAMs) in both amorphous and crystalline phases of TST are depicted in Fig. 17(d). In the amorphous phase, Ti atoms are positioned at the center of local octahedral arrangements, bonded to six Te atoms, thereby accounting for its exceptional crystallization speed. Compared to Sb_2Te_3, which displays a monotonical decrease in resistance, TST undergoes a significant resistance drop, as shown in Fig. 17(e), marking the crystallization temperatures (T_c) at $Ti_{0.32}Sb_2Te_3$, $Ti_{0.43}Sb_2Te_3$, and $Ti_{0.56}Sb_2Te_3$, occurring at 175.6, 185.5, and 195.9 °C, respectively. Fig. 17(f) demonstrates a gradual enhancement in ten-year data retention as Ti content increases. The 10-year data retention temperatures for $Ti_{0.32}Sb_2Te_3$, $Ti_{0.43}Sb_2Te_3$, and $Ti_{0.56}Sb_2Te_3$ are 79, 92, and 105 °C, respectively, with corresponding activation energies (E_a) of 2.1, 2.3, and 2.5 eV, respectively. Fig. 17(g) and (h) is the electrical performance of TST devices. TST can switch reversibly within 10 ns, and the endurance reaches 10^7, which means that TST maintains a good thermal performance while maintaining ultra-fast operating speed and fatigue performance.

In 2019, TST material was employed in a 4 Mb ePCM chip, as shown in Fig. 18. The programming time of the TST devices is as fast as 45 ns, which is increased by 80 % in programming speed compared with GST.

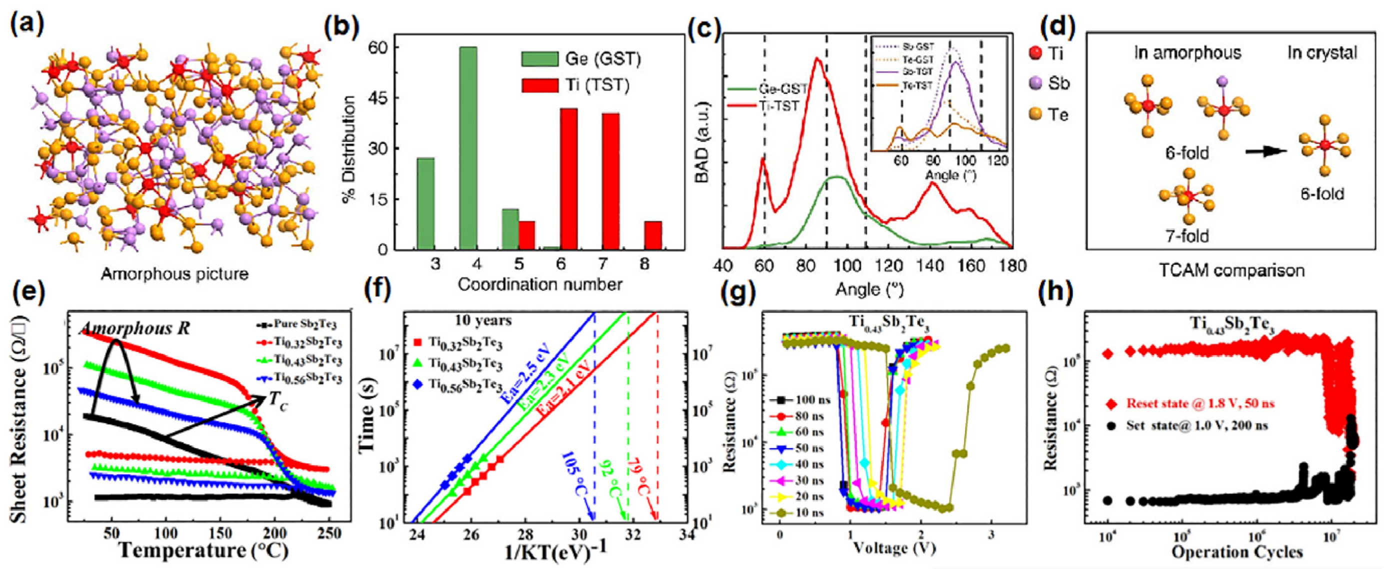

Fig. 17. The structural, thermal and electrical characteristics of TST. (a) The amorphous structure of TST. (b) The coordination number distribution of Ge and Ti in the respective amorphous model. (c) The bond angle distributions (BADs) around Ge in amorphous GST and Ti in amorphous TST. Inset shows the BADs around Sb and Te in amorphous GST and TST, respectively. (d) Proposed Ti-centered atomic motifs (TCAMs) in amorphous and crystalline TST. (e) Temperature dependence of the sheet resistance R_s of the Sb_2Te_3, and $Ti_xSb_2Te_3$ films. (f) The Arrhenius extrapolation at 10 years of data retention for $Ti_xSb_2Te_3$ films. (g) Resistance-voltage characteristics of PCM cell based on $Ti_{0.43}Sb_2Te_3$ material for different voltage pulse widths. (h) Cycling endurance characteristics of the PCM device based on $Ti_{0.43}Sb_2Te_3$ material. Copyright ©2014, Macmillan Publishers Limited. Copyright ©2015, American Chemical Society.

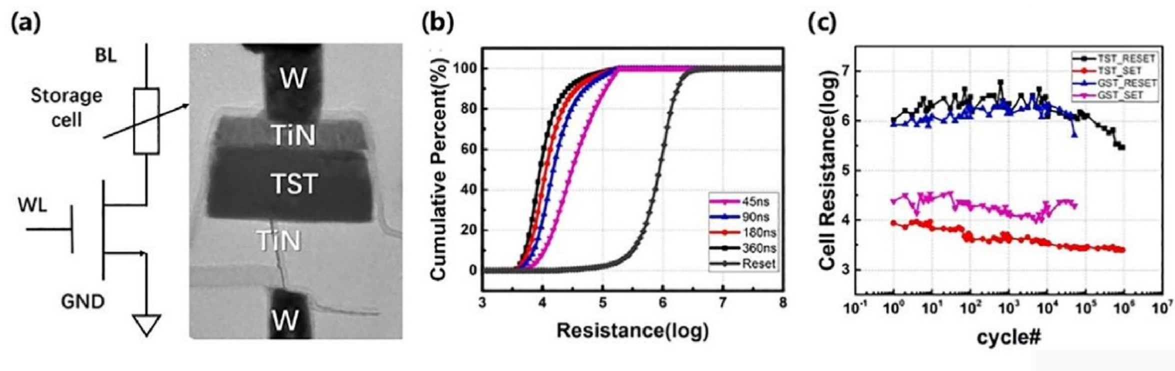

Fig. 18. PCM chip performances of TST. (a) 1T1R memory cell structure and TEM image of the blade-type PCM device. (b) The impact of Set pulse width on Set resistance distribution plot of PCM cells. The low resistance state (crystalline) can be reached within 45 ns. (c) Cycling endurance characteristics of the PCM device based on TST and GST material. Copyright ©2018 Elsevier Ltd.

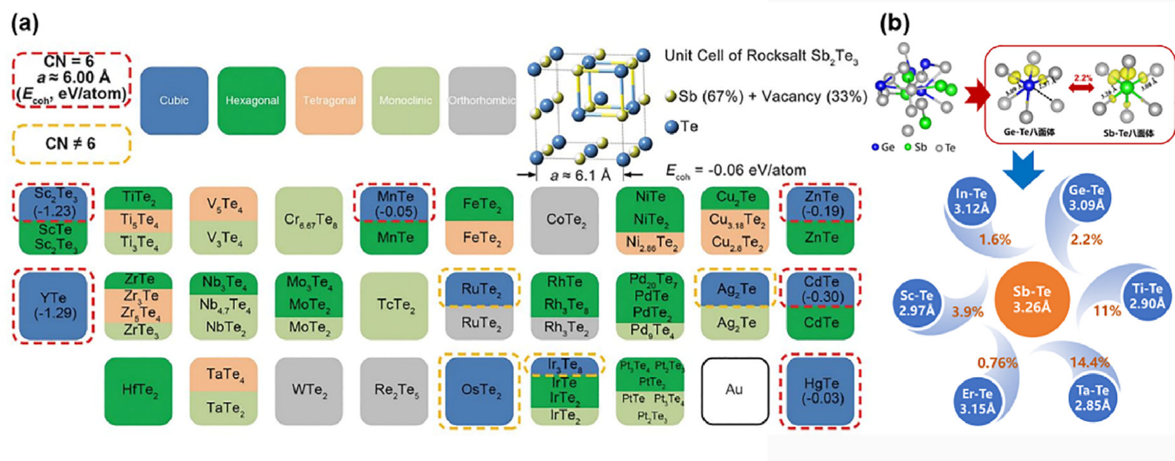

Fig. 19. Material screening based on the octahedral motifs. (a) The process and details of material screening grounded in the octahedral "gene" principle. (b) The lattice mismatch between A-Te (A is In, Ge, Ti, Ta, Er and Sc) and Sb-Te. Copyright ©2017, Science.

Table 2
Performance of the SST-based and GST-based PCM devices.

Phase-change material	GST	Ge-rich GST	CGST	TST	SST
T_c (°C)	~150	>185	>180	~186	~277
T_{10} (°C)	~85	~170	~128	~82	~169
E_a (eV)	~2.3	~4.3	~2.8	~2.3	~2.7
Speed (ns)	>30	>200	>100	>6	>100
Endurance	$>10^6$	$>10^8$	$>10^8$	$<10^7$	$<10^7$

Fig. 18(a) shows the schematic structure and cross-sectional TEM image of the device. Fig. 18(b) shows the change in resistance of TST at different pulse widths tested at 0.6 mA. Fig. 18(c) shows a comparison of the endurance of TST and GST-based PCM cell. The endurance of TST device is over 10^6 cycles, which is one order higher than the GST device.

The material screening mechanism grounded in the octahedral "gene" principle has been further refined, as illustrated in Fig. 19(a). In addition to the prerequisite that the amorphous structure already possesses six-coordinate octahedral motifs, the following criteria are also required: (1) the bond length should be close to 0.3 nm. (2) The melting temperature of the material should be greater than 900 K. (3) The introduction of impurities should not cause significant lattice distortion. (4) The crystalline state should be FCC structure and be able to maintain this structure for an extended period. (5) The dopant elements should be able to form stable chemical bonds with Te atoms and the resulting structure should also be FCC. Fig. 19(b) exhibits the extent of lattice mismatch for a selection of elements that meet the previously outlined screening conditions upon their incorporation into Sb_2Te_3 [41,130–133].

To compare the performance of GST, Ge-rich GST, CGST, TST and SST, the key characteristics, such as T_c, T_{10}, E_a, speed and endurance are listed in Table 2. Even though Sb_2Te_3 lacks outstanding device characteristics, the strategic incorporation of suitable elements can significantly enhance its thermal stability while preserving its rapid operational speed. Consequently, Sb_2Te_3 stands out as a highly promising material system that holds considerable potential for further research and exploration.

6. Conclusion

This paper provides an in-depth review of high thermal stability chalcogenide phase-change materials that are crucial for eNVM applications in next-generation non-volatile memory technologies. The key challenge for ePCM is the thermal stability for reliable performance after high temperature treatments. Material engineering strategies to address this challenge are discussed, including the optimization of Ge-rich GST materials, the doping of GST materials with light elements, and the binary Sb_2Te_3 alloys with titanium, silicon, and scandium dopants. These advancements have led to improvement of thermal stability, data retention, and cycling endurance of phase-change material, making PCMs a promising candidate for automotive MCU and embedded memory applications. The industrialization state of these materials and their impact on the future development of ePCM technologies are also demonstrated. Doping carbon in the Ge-rich GST alloy might be a feasible

way to further improve the thermal stability and reliability of ePCM. The continuation and expansion of high thermal stability chalcogenide phase-change material investigations are essential to ensure PCM chips with improved properties for embedded data storage applications.

CRediT authorship contribution statement

Ruobing Wang: Writing – original draft, Investigation, Formal analysis, Data curation. **Ziqi Wan:** Writing – original draft, Investigation, Data curation. **Xixi Zou:** Writing – original draft, Investigation, Data curation. **Shanwen Chen:** Writing – original draft, Investigation, Data curation. **Sannian Song:** Writing – review & editing, Visualization, Data curation. **Xilin Zhou:** Writing – review & editing, Supervision, Project administration, Funding acquisition, Conceptualization. **Zhitang Song:** Writing – review & editing, Supervision, Project administration, Funding acquisition.

Declaration of competing interest

The authors declare that they have no known competing financial interests or personal relationships that could have appeared to influence the work reported in this paper.

Acknowledgments

This work was financially supported by the National Key Research and Development Program of China (2023YFB4404500), the Strategic Priority Research Program of the Chinese Academy of Sciences (XDB0670000), the National Natural Science Foundation of China (92164302, 62404233, 62174168), Science and Technology Council of Shanghai (23JC1400900, 24YF2754700), the Autonomous Deployment Project of State Key Laboratory of Materials for Integrated Circuits (No. SKLJC- Z2024-A01), China Postdoctoral Science Foundation (2023TQ0363 and 2024M753370), and the Postdoctoral Fellowship Program of CPSF (GZC20232839).

References

[1] C.-W. Yoon, The Fundamentals of NAND Flash Memory: technology for tomorrow's fourth industrial revolution, IEEE Solid-State Circuits Mag 14 (2022) 56–65, https://doi.org/10.1109/MSSC.2022.3166466.

[2] A. Belmonte, H. Oh, N. Rassoul, G.L. Donadio, J. Mitard, H. Dekkers, R. Delhougne, S. Subhechha, A. Chasin, M.J. van Setten, L. Kljucar, M. Mao, H. Puliyalil, M. Pak, L. Teugels, D. Tsvetanova, K. Banerjee, L. Souriau, Z. Tokei, L. Goux, G.S. Kar, Capacitor-less, Long-Retention (>400s) DRAM Cell Paving the Way towards Low-Power and High-Density Monolithic 3D DRAM, in: 2020, IEEE Int. Electron Devices Meet. IEDM, 2020, pp. 28.2.1–28.2.4, https://doi.org/10.1109/IEDM13553.2020.9371900.

[3] M. Marinella, The future of memory, in: 2013 IEEE Aerosp, . Conf., 2013, pp. 1–11, https://doi.org/10.1109/AERO.2013.6507427.

[4] R.F. Freitas, W.W. Wilcke, Storage-class memory: the next storage system technology, IBM J. Res. Dev. 52 (2008) 439–447, https://doi.org/10.1147/rd.524.0439.

[5] R. Bez, A. Pirovano, 1 - overview of non-volatile memory technology: markets, technologies and trends, in: Y. Nishi (Ed.), Adv. Non-volatile Mem. Storage Technol., Woodhead Publishing, 2014, pp. 1–24, https://doi.org/10.1533/9780857098092.1.

[6] M.L. Gallo, A. Sebastian, An overview of phase-change memory device physics, J. Phys. Appl. Phys. 53 (2020) 213002, https://doi.org/10.1088/1361-6463/ab7794.

[7] H.-Y. Cheng, F. Carta, W.-C. Chien, H.-L. Lung, M.J. BrightSky, 3D cross-point phase-change memory for storage-class memory, J. Phys. Appl. Phys. 52 (2019) 473002, https://doi.org/10.1088/1361-6463/ab39a0.

[8] J. Yang, B. Li, D.J. Lilja, Exploring performance characteristics of the Optane 3D Xpoint storage technology, ACM Trans. Model. Perform. Eval. Comput. Syst. 5 (4) (2020) 1–4:28, https://doi.org/10.1145/3372783.

[9] M. Hellenbrand, I. Teck, J.L. MacManus-Driscoll, Progress of emerging non-volatile memory technologies in industry, MRS Commun (2024), https://doi.org/10.1557/s43579-024-00660-2.

[10] P. Cappelletti, J. Slaughter, 6 - embedded memory solutions: charge storage based, resistive and magnetic, in: A. Redaelli, F. Pellizzer (Eds.), Semicond. Mem. Syst., Woodhead Publishing, 2022, pp. 159–215, https://doi.org/10.1016/B978-0-12-820758-1.00007-8.

[11] K.-J. Lee, B.-H. Cho, W.-Y. Cho, S. Kang, B.-G. Choi, H.-R. Oh, C.-S. Lee, H.-J. Kim, J.-M. Park, Q. Wang, M.-H. Park, Y.-H. Ro, J.-Y. Choi, K.-S. Kim, Y.-R. Kim, I.-C. Shin, K.-W. Lim, H.-K. Cho, C.-H. Choi, W.-R. Chung, D.-E. Kim, Y.-J. Yoon, K.-S. Yu, G.-T. Jeong, H.-S. Jeong, C.-K. Kwak, C.-H. Kim, K. Kim, A 90 nm 1.8 V 512 Mb diode-switch PRAM with 266 MB/s read throughput, IEEE J. Solid-State Circuits 43 (2008) 150–162, https://doi.org/10.1109/JSSC.2007.908001.

[12] G.W. Burr, M.J. Breitwisch, M. Franceschini, D. Garetto, K. Gopalakrishnan, B. Jackson, B. Kurdi, C. Lam, L.A. Lastras, A. Padilla, B. Rajendran, S. Raoux, R.S. Shenoy, Phase change memory technology, J. Vac. Sci. Technol. B Nanotechnol. Microelectron. Mater. Process. Meas. Phenom. 28 (2010) 223–262, https://doi.org/10.1116/1.3301579.

[13] H. Wang, Challenges in automotive memory solutions, in: 2018 IEEE Int. Mem. Workshop IMW, 2018, pp. 1–7, https://doi.org/10.1109/IMW.2018.8388782.

[14] P. Cappelletti, R. Annunziata, F. Arnaud, F. Disegni, A. Maurelli, P. Zuliani, Phase change memory for automotive grade embedded NVM applications, J. Phys. Appl. Phys. 53 (2020) 193002, https://doi.org/10.1088/1361-6463/ab71aa.

[15] A. Faraclas, N. Williams, A. Gokirmak, H. Silva, Modeling of Set and Reset operations of phase-change memory cells, IEEE Electron Device Lett. 32 (2011) 1737–1739, https://doi.org/10.1109/LED.2011.2168374.

[16] S. Ghazi Sarwat, T.M. Philip, C.-T. Chen, B. Kersting, R.L. Bruce, C.-W. Cheng, N. Li, N. Saulnier, M. BrightSky, A. Sebastian, Projected mushroom type phase-change memory, Adv. Funct. Mater. 31 (2021) 2106547, https://doi.org/10.1002/adfm.202106547.

[17] J.Y. Wu, M. Breitwisch, S. Kim, T.H. Hsu, R. Cheek, P.Y. Du, J. Li, E.K. Lai, Y. Zhu, T.Y. Wang, H.Y. Cheng, A. Schrott, E.A. Joseph, R. Dasaka, S. Raoux, M.H. Lee, H.L. Lung, C. Lam, A low power phase change memory using thermally confined TaN/TiN bottom electrode, in: 2011 Int. Electron Devices Meet, 2011, pp. 3.2.1–3.2.4, https://doi.org/10.1109/IEDM.2011.6131479.

[18] G. Servalli, A 45nm generation phase change memory technology, in: 2009 IEEE Int. Electron Devices Meet, IEDM, 2009, pp. 1–4, https://doi.org/10.1109/IEDM.2009.5424409.

[19] F. Pellizzer, A. Pirovano, F. Ottogalli, M. Magistretti, M. Scaravaggi, P. Zuliani, M. Tosi, A. Benvenuti, P. Besana, S. Cadeo, T. Marangon, R. Morandi, R. Piva, A. Spandre, R. Zonca, A. Modelli, E. Varesi, T. Lowrey, A. Lacaita, G. Casagrande, P. Cappelletti, R. Bez, Novel/spl mu/trench phase-change memory cell for embedded and stand-alone non-volatile memory applications, in: Dig. Tech. Pap. 2004 Symp. VLSI Technol., 2004, 2004, pp. 18–19, https://doi.org/10.1109/VLSIT.2004.1345368.

[20] P. Zuliani, E. Varesi, E. Palumbo, M. Borghi, I. Tortorelli, D. Erbetta, G.D. Libera, N. Pessina, A. Gandolfo, C. Prelini, L. Ravazzi, R. Annunziata, Overcoming Temperature Limitations in Phase Change Memories with Optimized $Ge_xSb_yTe_z$, IEEE Trans. Electron Devices 60 (2013) 4020–4026, https://doi.org/10.1109/TED.2013.2285403.

[21] S.R. Ovshinsky, Reversible electrical switching phenomena in disordered structures, Phys. Rev. Lett. 21 (1968) 1450–1453, https://doi.org/10.1103/PhysRevLett.21.1450.

[22] N. Yamada, Development of materials for third generation optical storage media, in: S. Raoux, M. Wuttig (Eds.), Phase Change Mater, Springer US, Boston, MA, 2009, pp. 199–226, https://doi.org/10.1007/978-0-387-84874-7_10.

[23] J.P. Perdew, Y. Wang, Accurate and simple analytic representation of the electron-gas correlation energy, Phys. Rev. B 45 (1992) 13244–13249, https://doi.org/10.1103/PhysRevB.45.13244.

[24] M. Chen, K.A. Rubin, R.W. Barton, Compound materials for reversible, phase-change optical data storage, Appl. Phys. Lett. 49 (1986) 502–504, https://doi.org/10.1063/1.97617.

[25] L. Perniola, V. Sousa, A. Fantini, E. Arbaoui, A. Bastard, M. Armand, A. Fargeix, C. Jahan, J.-F. Nodin, A. Persico, D. Blachier, A. Toffoli, S. Loubriat, E. Gourvest, G. Betti Beneventi, H. Feldis, S. Maitrejean, S. Lhostis, A. Roule, O. Cueto, G. Reimbold, L. Poupinet, T. Billon, B. De Salvo, D. Bensahel, P. Mazoyer, R. Annunziata, P. Zuliani, F. Boulanger, Electrical behavior of phase-change memory cells based on GeTe, IEEE Electron Device Lett. 31 (2010) 488–490, https://doi.org/10.1109/LED.2010.2044136.

[26] K. Singh, S. Kumari, H. Singh, N. Bala, P. Singh, A. Kumar, A. Thakur, A review on GeTe thin film-based phase-change materials, Appl. Nanosci. 13 (2023) 95–110, https://doi.org/10.1007/s13204-021-01911-7.

[27] P. Arun, A.G. Vedeshwar, N.C. Mehra, Laser-induced crystallization in amorphous films of (C = S, Se, Te), potential optical storage media, J. Phys. Appl. Phys. 32 (1999) 183.

[28] N. Yamada, E. Ohno, N. Akahira, K. Nishiuchi, K. Nagata, M. Takao, High speed overwritable phase change optical disk material, Jpn. J. Appl. Phys. 26 (1987) 61, https://doi.org/10.7567/JJAPS.26S4.61.

[29] S. Guerin, B. Hayden, D.W. Hewak, C. Vian, Synthesis and screening of phase change chalcogenide thin film materials for data storage, ACS Comb. Sci. 19 (2017) 478–491, https://doi.org/10.1021/acscombsci.7b00047.

[30] N. Yamada, E. Ohno, K. Nishiuchi, N. Akahira, M. Takao, Rapid-phase transitions of GeTe-Sb_2Te_3 pseudobinary amorphous thin films for an optical disk memory, J. Appl. Phys. 69 (1991) 2849–2856, https://doi.org/10.1063/1.348620.

[31] F. Ottogalli, A. Pirovano, F. Pellizzer, M. Tosi, P. Zuliani, P. Bonetalli, R. Bez, Phase-change memory technology for embedded applications, in: Proc. 30th Eur. Solid-State Circuits Conf. IEEE Cat No04EX850, 2004, pp. 293–296, https://doi.org/10.1109/ESSDER.2004.1356547.

[32] N. Yamada, T. Matsunaga, Structure of laser-crystallized $Ge_2Sb_{2+x}Te_5$ sputtered thin films for use in optical memory, J. Appl. Phys. 88 (2000) 7020–7028, https://doi.org/10.1063/1.1314323.

[33] B. Zhang, W. Zhang, Z. Shen, Y. Chen, J. Li, S. Zhang, Z. Zhang, M. Wuttig, R. Mazzarello, E. Ma, X. Han, Element-resolved atomic structure imaging of

rocksalt $Ge_2Sb_2Te_5$ phase-change material, Appl. Phys. Lett. 108 (2016) 191902, https://doi.org/10.1063/1.4949011.
[34] M. Xu, S.-J. Wei, S. Wu, F. Pei, J. Li, S.-Y. Wang, L.-Y. Chen, Y. Jia, Theoretical and experimental investigations of the optical properties of $Ge_2Sb_2Te_5$ for multi-state optical data storage, J. Korean Phys. Soc. 53 (2008) 2265–2269, https://doi.org/10.3938/jkps.53.2265.
[35] M. Zhu, O. Cojocaru-Mirédin, A.M. Mio, J. Keutgen, M. Küpers, Y. Yu, J.-Y. Cho, R. Dronskowski, M. Wuttig, Unique bond breaking in crystalline phase change materials and the quest for metavalent bonding, Adv. Mater. 30 (2018) 1706735, https://doi.org/10.1002/adma.201706735.
[36] B.J. Kooi, M. Wuttig, Chalcogenides by design: functionality through metavalent bonding and confinement, Adv. Mater. 32 (2020) 1908302, https://doi.org/10.1002/adma.201908302.
[37] A. Fantini, L. Perniola, M. Armand, J.F. Nodin, V. Sousa, A. Persico, J. Cluzel, C. Jahan, S. Maitrejean, S. Lhostis, A. Roule, C. Dressler, G. Reimbold, B. De Salvo, P. Mazoyer, D. Bensahel, F. Boulanger, Comparative assessment of GST and GeTe materials for application to embedded phase-change memory devices, in: 2009 IEEE Int. Mem, Workshop, 2009, pp. 1–2, https://doi.org/10.1109/IMW.2009.5090585.
[38] N. Ciocchini, E. Palumbo, M. Borghi, P. Zuliani, R. Annunziata, D. Ielmini, Unified Reliability Modeling of Ge-Rich Phase Change Memory for Embedded Applications, in: 2013, IEEE Int. Electron Devices Meet, 2013, pp. 22.1.1–22.1.4, https://doi.org/10.1109/IEDM.2013.6724681.
[39] Z.T. Song, D.L. Cai, X. Li, L. Wang, Y.F. Chen, H.P. Chen, Q. Wang, Y.P. Zhan, M.H. Ji, High Endurance Phase Change Memory Chip Implemented Based on Carbon-Doped $Ge_2Sb_2Te_5$ in 40 Nm Node for Embedded Application, in: 2018, IEEE Int. Electron Devices Meet. IEDM, 2018, pp. 27.5.1–27.5.4, https://doi.org/10.1109/IEDM.2018.8614538.
[40] F. Rao, Z. Song, K. Ren, X. Zhou, Y. Cheng, L. Wu, B. Liu, Si–Sb–Te materials for phase change memory applications, Nanotechnology 22 (2011) 145702, https://doi.org/10.1088/0957-4484/22/14/145702.
[41] M. Zhu, M. Xia, F. Rao, X. Li, L. Wu, X. Ji, S. Lv, Z. Song, S. Feng, H. Sun, S. Zhang, One order of magnitude faster phase change at reduced power in Ti-Sb-Te, Nat. Commun. 5 (2014) 4086, https://doi.org/10.1038/ncomms5086.
[42] S. Sun, X. Wang, Y. Jiang, Y. Lei, S. Zhang, S. Kumar, J. Zhang, E. Ma, R. Mazzarello, J.-J. Wang, W. Zhang, High-throughput screening to identify two-dimensional layered phase-change chalcogenides for embedded memory applications, npj Comput. Mater. 10 (2024) 1–10, https://doi.org/10.1038/s41524-024-01387-3.
[43] R. Annunziata, P. Zuliani, M. Borghi, G. De Sandre, L. Scotti, C. Prelini, M. Tosi, I. Tortorelli, F. Pellizzer, Phase Change Memory Technology for Embedded Non Volatile Memory Applications for 90nm and beyond, in: 2009, IEEE Int. Electron Devices Meet. IEDM, 2009, pp. 1–4, https://doi.org/10.1109/IEDM.2009.5424413.
[44] N. Ciocchini, E. Palumbo, M. Borghi, P. Zuliani, R. Annunziata, D. Ielmini, Unified Reliability Modeling of Ge-Rich Phase Change Memory for Embedded Applications, in: 2013, IEEE Int. Electron Devices Meet, 2013, pp. 22.1.1–22.1.4, https://doi.org/10.1109/IEDM.2013.6724681.
[45] V. Sousa, G. Navarro, N. Castellani, M. Coue, O. Cueto, C. Sabbione, P. Noe, L. Perniola, S. Blonkowski, P. Zuliani, R. Annunziata, Operation fundamentals in 12Mb Phase Change Memory based on innovative Ge-rich GST materials featuring high reliability performance, in: 2015 Symp. VLSI Technol. VLSI Technol, IEEE, Kyoto, Japan, 2015, pp. T98–T99, https://doi.org/10.1109/VLSIT.2015.7223708.
[46] N. Ciocchini, E. Palumbo, M. Borghi, P. Zuliani, R. Annunziata, D. Ielmini, Modeling resistance instabilities of Set and Reset states in phase change memory with Ge-rich GeSbTe, IEEE Trans. Electron Devices 61 (2014) 2136–2144, https://doi.org/10.1109/TED.2014.2313889.
[47] H.Y. Cheng, T.H. Hsu, S. Raoux, J.Y. Wu, P.Y. Du, M. Breitwisch, Y. Zhu, E.K. Lai, E. Joseph, S. Mittal, R. Cheek, A. Schrott, S.C. Lai, H.L. Lung, C. Lam, A high performance phase change memory with fast switching speed and high temperature retention by engineering the $Ge_xSb_yTe_z$ phase change material, in: 2011 Int. Electron Devices Meet, 2011, pp. 3.4.1–3.4.4, https://doi.org/10.1109/IEDM.2011.6131481.
[48] P. Zuliani, E. Varesi, E. Palumbo, M. Borghi, I. Tortorelli, D. Erbetta, G.D. Libera, N. Pessina, A. Gandolfo, C. Prelini, L. Ravazzi, R. Annunziata, Overcoming temperature limitations in phase change memories with optimized $Ge_xSb_yTe_z$, IEEE Trans. ELECTRON DEVICES 60 (2013).
[49] E. Palumbo, P. Zuliani, M. Borghi, R. Annunziata, Forming operation in Ge-rich $Ge_xSb_yTe_z$ phase change memories, Solid State Electron. 133 (2017) 38–44, https://doi.org/10.1016/j.sse.2017.03.016.
[50] J. Akola, R.O. Jones, Structural phase transitions on the nanoscale: the crucial pattern in the phase-change materials $Ge_2Sb_2Te_5$ and GeTe, Phys. Rev. B 76 (2007) 235201, https://doi.org/10.1103/PhysRevB.76.235201.
[51] J. Kluge, G. Navarro, V. Sousa, N. Castellani, S. Blonkowski, R. Annunziata, P. Zuliani, L. Perniola, High operating temperature reliability of optimized Ge-rich GST wall PCM devices, in: 2016 IEEE 8th Int. Mem. Workshop IMW, IEEE, Paris, France, 2016, pp. 1–4, https://doi.org/10.1109/IMW.2016.7495273.
[52] L. Henry, N. Bernier, M. Jacob, G. Navarro, L. Clément, J.-L. Rouvière, E. Robin, Studying phase change memory devices by coupling scanning precession electron diffraction and energy dispersive X-ray analysis, Acta Mater. 201 (2020) 72–78, https://doi.org/10.1016/j.actamat.2020.09.033.
[53] M. Agati, F. Renaud, D. Benoit, A. Claverie, In-situ transmission electron microscopy studie of the crystallization of N-doped Ge-rich GeSbTe materials, MRS Commun 8 (2018) 1145–1152, https://doi.org/10.1557/mrc.2018.168.
[54] S.M.S. Privitera, I. López García, C. Bongiorno, V. Sousa, M.C. Cyrille, G. Navarro, C. Sabbione, E. Carria, E. Rimini, Crystallization properties of melt-quenched Ge-rich GeSbTe thin films for phase change memory applications, J. Appl. Phys. 128 (2020) 155105, https://doi.org/10.1063/5.0023696.
[55] E. Rahier, S. Ran, N. Ratel Ramond, S. Ma, L. Calmels, S. Saha, C. Mocuta, D. Benoit, Y. Le Friec, M.A. Luong, A. Claverie, Crystallization of Ge-rich GeSbTe alloys: the riddle is solved, ACS Appl. Electron. Mater. 4 (2022) 2682–2688, https://doi.org/10.1021/acsaelm.2c00038.
[56] J. Remondina, Exploring the evolution of mass density and thickness of N-doped Ge-rich GeSbTe during multistep crystallization, Sci. Rep. (2024).
[57] M.A. Luong, M. Agati, N. Ratel Ramond, J. Grisolia, Y. Le Friec, D. Benoit, A. Claverie, On some unique specificities of Ge-rich GeSbTe phase-change material alloys for nonvolatile embedded-memory applications, Phys. Status Solidi RRL – Rapid Res. Lett. 15 (2021) 2000471, https://doi.org/10.1002/pssr.202000471.
[58] M. Pasotti, R. Zurla, M. Carissimi, C. Auricchio, D. Brambilla, E. Calvetti, L. Capecchi, L. Croce, D. Gallinari, C. Mazzaglia, V. Rana, A. Cabrini, G. Torelli, A 32-KB ePCM for real-time data processing in automotive and smart power applications, IEEE J. Solid-State Circuits 53 (2018) 2114–2125, https://doi.org/10.1109/JSSC.2018.2828805.
[59] M. Pasotti, M. Carissimi, C. Auricchio, D. Brambilla, E. Calvetti, L. Capecchi, L. Croce, D. Gallinari, C. Mazzaglia, V. Rana, R. Zurla, A. Cabrini, G. Torelli, A 32KB 18ns random access time embedded PCM with enhanced program throughput for automotive and smart power applications, in: ESSCIRC 2017 - 43rd IEEE Eur. Solid State Circuits Conf, IEEE, Leuven, 2017, pp. 320–323, https://doi.org/10.1109/ESSCIRC.2017.8094590.
[60] R. Ranica, R. Berthelon, A. Gandolfo, G. Samanni, E. Gomiero, J. Jasse, P. Mattavelli, J. Sandrini, M. Querre, Y. Le-Friec, J. Poulet, V. Caubet, L. Favennec, C. Boccaccio, G. Ghezzi, C. Gallon, Jc Grenier, B. Dumont, O. Weber, A. Villaret, R. Beneyton, N. Cherault, D. Ristoiu, S. Del Medico, O. Kermarrec, Jp Reynard, P. Boivin, A. Souhaite, L. Desvoivres, S. Chouteau, Po Sassoulas, L. Clement, A. Valery, E. Petroni, D. Turgis, A. Lippiello, L. Scotti, F. Disegni, A. Ventre, D. Ornaghi, M. De Tomasi, A. Maurelli, A. Conte, F. Arnaud, A. Redaelli, R. Annunziata, P. Cappelletti, F. Piazza, P. Ferreira, R. Gonella, E. Ciantar, Heater system optimization for robust ePCM reliability and scalability in 28nm FDSOI technology, in: 2021 IEEE Int. Electron Devices Meet. IEDM, IEEE, San Francisco, CA, USA, 2021, pp. 28.1.1–28.1.4, https://doi.org/10.1109/IEDM19574.2021.9720669.
[61] F. Arnaud, P. Zuliani, J.P. Reynard, A. Gandolfo, F. Disegni, P. Mattavelli, E. Gomiero, G. Samanni, C. Jahan, R. Berthelon, O. Weber, E. Richard, V. Barral, A. Villaret, S. Kohler, J.C. Grenier, R. Ranica, C. Gallon, A. Souhaite, D. Ristoiu, L. Favennec, V. Caubet, S. Delmedico, N. Cherault, R. Beneyton, S. Chouteau, P.O. Sassoulas, A. Vernhet, Y. Le Friec, F. Domengie, L. Scotti, D. Pacelli, J.L. Ogier, F. Boucard, S. Lagrasta, D. Benoit, L. Clement, P. Boivin, P. Ferreira, R. Annunziata, P. Cappelletti, Truly innovative 28nm FDSOI technology for automotive micro-controller applications embedding 16MB phase change memory, in: 2018 IEEE Int. Electron Devices Meet. IEDM, IEEE, San Francisco, CA, 2018, pp. 18.4.1–18.4.4, https://doi.org/10.1109/IEDM.2018.8614595.
[62] P. Cappelletti, J. Slaughter, Embedded memory solutions: charge storage based, resistive and magnetic, in: Semicond. Mem. Syst., Elsevier, 2022, pp. 159–215, https://doi.org/10.1016/B978-0-12-820758-1.00007-8.
[63] F. Arnaud, P. Ferreira, F. Piazza, A. Gandolfo, P. Zuliani, P. Mattavelli, E. Gomiero, G. Samanni, J. Jasse, C. Jahan, J.P. Reynard, R. Berthelon, O. Weber, A. Villaret, B. Dumont, J.C. Grenier, R. Ranica, C. Gallon, C. Boccaccio, A. Souhaite, L. Desvoivres, D. Ristoiu, L. Favennec, V. Caubet, S. Delmedico, N. Cherault, R. Beneyton, S. Chouteau, P.O. Sassoulas, L. Clement, P. Boivin, D. Turgis, F. Disegni, J.L. Ogier, X. Federspiel, O. Kermarrec, M. Molgg, A. Viscuso, R. Annunziata, A. Maurelli, P. Cappelletti, E. Ciantar, High Density Embedded PCM Cell in 28nm FDSOI Technology for Automotive Micro-controller Applications, in: 2020, IEEE Int. Electron Devices Meet. IEDM, IEEE, San Francisco, CA, USA, 2020, pp. 24.2.1–24.2.4, https://doi.org/10.1109/IEDM13553.2020.9371934.
[64] D. Min, J. Park, O. Weber, F. Wacquant, A. Villaret, E. Vandenbossche, F. Arnaud, E. Bernard, S. Elghouli, C. Boccaccio, L. Favennec, R. Gonella, J. Galvier, J. Yun, J. Park, M. Lee, P. Yoon, I. Lee, H. Seo, H. Choi, C. Oh, J. Kang, S. Park, H. Lee, Y. Choi, I. Kim, J. Jo, Y. Park, J. Park, Y. Lee, J. Jung, J. Lee, H. Jang, J. Kang, J. Kwon, J. Kim, S. Maeda, Y. Hong, 18nm FDSOI technology platform embedding PCM & innovative continuous-active construct enhancing performance for leading-edge MCU applications, in: 2021 IEEE Int. Electron Devices Meet. IEDM, IEEE, San Francisco, CA, USA, 2021, pp. 13.1.1–13.1.4, https://doi.org/10.1109/IEDM19574.2021.9720542.
[65] A. Conte, F. Tomaiuolo, M. Ruta, A. Redaelli, F. Arnaud, T. Jouanneau, C. Boccaccio, O. Weber, An 18nm ePCM with BJT selector NVM design for advanced microcontroller applications, in: 2023 IEEE Int. Mem. Workshop IMW, IEEE, Monterey, CA, USA, 2023, pp. 1–4, https://doi.org/10.1109/IMW56887.2023.10145983.
[66] M. Agati, M. Vallet, S. Joulié, D. Benoit, A. Claverie, Chemical phase segregation during the crystallization of Ge-rich GeSbTe alloys, J. Mater. Chem. C 7 (2019) 8720–8729, https://doi.org/10.1039/C9TC02302J.
[67] E. Palumbo, P. Zuliani, M. Borghi, R. Annunziata, Forming operation in Ge-rich Ge x Sb y Te z phase change memories, Solid State Electron. 133 (2017) 38–44, https://doi.org/10.1016/j.sse.2017.03.016.
[68] G. Navarro, M. Coue, A. Kiouseloglou, P. Noe, F. Fillot, V. Delaye, A. Persico, A. Roule, M. Bernard, C. Sabbione, D. Blachier, V. Sousa, L. Perniola, S. Maitrejean, A. Cabrini, G. Torelli, P. Zuliani, R. Annunziata, E. Palumbo, M. Borghi, G. Reimbold, B. De Salvo, Trade-off between SET and data retention performance thanks to innovative materials for phase-change memory, in: 2013 IEEE Int. Electron Devices Meet, IEEE, Washington, DC, USA, 2013, pp. 21.5.1–21.5.4, https://doi.org/10.1109/IEDM.2013.6724678.

[69] L. Laurin, M. Baldo, E. Petroni, G. Samanni, L. Turconi, A. Motta, M. Borghi, A. Serafini, D. Codegoni, M. Scuderi, S. Ran, A. Claverie, D. Ielmini, R. Annunziata, A. Redaelli, Unveiling retention physical mechanism of Ge-rich GST ePCM technology, in: 2023 IEEE Int. Reliab. Phys. Symp. IRPS, IEEE, Monterey, CA, USA, 2023, pp. 1–7, https://doi.org/10.1109/IRPS48203.2023.10118155.

[70] M.A. Luong, D. Wen, E. Rahier, N.R. Ramond, B. Pecassou, Y.L. Friec, D. Benoit, A. Claverie, Impact of nitrogen on the crystallization and microstructure of Ge-rich GeSbTe alloys, Phys. Status Solidi RRL (2021).

[71] O. Daoudi, E. Nolot, Y. Mazel, M. Dupraz, H. Roussel, F. Fillot, V.-H. Le, M. Dartois, M. Tessaire, H. Renevier, G. Navarro, The effects of Sb/Te ratio on crystallization kinetics in Ge-rich GeSbTe phase-change materials, J. Appl. Phys. 136 (2024) 155105, https://doi.org/10.1063/5.0221206.

[72] E. Palumbo, A. Motta, E. Petroni, D. Gallinari, A. Gilardini, A. Galbiati, M. Borghi, R. Annunziata, A. Redaelli, ePCM reliability improvement through active material carbon implantation, in: ESSDERC 2023 - IEEE 53rd Eur. Solid-State Device Res. Conf. ESSDERC, IEEE, Lisbon, Portugal, 2023, pp. 29–32, https://doi.org/10.1109/ESSDERC59256.2023.10268520.

[73] Y. Canvel, S. Lagrasta, C. Boixaderas, S. Barnola, Y. Mazel, E. Martinez, Study of Ge-rich GeSbTe etching process with different halogen plasmas, J. Vac. Sci. Technol. Vac. Surf. Films 37 (2019) 031302, https://doi.org/10.1116/1.5089037.

[74] E. Gomiero, D. Ristoiu, J.P. Reynard, L. Clement, P. Zuliani, R. Annunziata, F. Arnaud, G. Samanni, J. Jasse, C. Jahan, O. Weber, R. Berthelon, R. Ranica, L. Favennec, V. Caubet, Crystallization speed in Ge-rich PCM cells as a function of process and programming conditions, IEEE J. Electron Devices Soc. 7 (2019) 517–521, https://doi.org/10.1109/JEDS.2019.2913467.

[75] F. Yang, X. Tang, T. Chen, M. Wang, L. Zhang, J. Han, L. Wan, D. Ke, Y. Dai, Effect of Si doping on the structure and optical properties of $Ge_2Sb_2Te_5$ studied by ab initio calculations, Comput. Mater. Sci. 168 (2019) 253–259, https://doi.org/10.1016/j.commatsci.2019.05.019.

[76] Y. Ling, Y. Lin, B. Qiao, Y. Lai, J. Feng, T. Tang, B. Cai, B. Chen, Effects of Si doping on phase transition of Ge_2 Sb_2 Te_5 films by in situ resistance measurements, Jpn. J. Appl. Phys. 45 (2006) L349, https://doi.org/10.1143/JJAP.45.L349.

[77] J. Feng, Y. Zhang, B.W. Qiao, Y.F. Lai, Y.Y. Lin, B.C. Cai, T.A. Tang, B. Chen, Si doping in Ge2Sb2Te5 film to reduce the writing current of phase change memory, Appl. Phys. A 87 (2007) 57–62, https://doi.org/10.1007/s00339-006-3851-2.

[78] Y. Xue, S. Song, X. Chen, S. Yan, S. Lv, T. Xin, Z. Song, Enhanced performance of phase change memory by grain size reduction, J. Mater. Chem. C 10 (2022) 3585–3592, https://doi.org/10.1039/D1TC06045G.

[79] Y. Kim, U. Hwang, Y.J. Cho, H.M. Park, M.-H. Cho, P.-S. Cho, J.-H. Lee, Change in electrical resistance and thermal stability of nitrogen incorporated Ge2Sb2Te5 films, Appl. Phys. Lett. 90 (2007) 021908, https://doi.org/10.1063/1.2431462.

[80] K. Do, D. Lee, J.-H. Bae, D.-H. Ko, H. Sohn, M.-H. Cho, Comparison of the crystallization behaviors in as-deposited and melt-quenched N-doped Ge2Sb2Te5 thin films, J. Electrochem. Soc. 158 (2011) H347, https://doi.org/10.1149/1.3543927.

[81] B. Liu, Z. Song, T. Zhang, J. Xia, S. Feng, B. Chen, Effect of N-implantation on the structural and electrical characteristics of Ge2Sb2Te5 phase change film, Thin Solid Films 478 (2005) 49–55, https://doi.org/10.1016/j.tsf.2004.09.057.

[82] J. Shen, T. Li, X. Chen, S. Jia, S. Lv, L. Li, Z. Song, M. Zhu, Dynamic evolution of thermally induced element distribution in nitrogen modified phase change materials, J. Appl. Phys. 128 (2020) 075701, https://doi.org/10.1063/5.0006519.

[83] D. Gao, B. Liu, Z. Xu, Y. Li, L. Wang, Z. Song, N. Zhu, Y. Zhan, S. Feng, Failure analysis of nitrogen-doped Ge_2 Sb_2 Te_5 phase change memory, IEEE Trans. Device Mater. Reliab. 16 (2016) 74–79, https://doi.org/10.1109/TDMR.2016.2520984.

[84] Z. Xu, B. Liu, Y. Chen, Z. Zhang, D. Gao, H. Wang, Z. Song, C. Wang, J. Ren, N. Zhu, Y. Xiang, Y. Zhan, S. Feng, The improvement of nitrogen doped Ge 2 Sb 2 Te 5 on the phase change memory resistance distributions, Solid State Electron. 116 (2016) 119–123, https://doi.org/10.1016/j.sse.2015.11.001.

[85] M.H. Jang, S.J. Park, D.H. Lim, S.J. Park, M.-H. Cho, S.J. Cho, Y.H. Cho, J.-H. Lee, Effects of oxygen incorporation in GeSbTe films on electrical properties and thermal stability, Appl. Phys. Lett. 96 (2010) 092108, https://doi.org/10.1063/1.3353973.

[86] M.H. Jang, S.J. Park, D.H. Lim, S.J. Park, M.-H. Cho, D.-H. Ko, S.J. Cho, The phase change effect of oxygen-incorporation in GeSbTe films, J. Electrochem. Soc. 158 (2011) H471, https://doi.org/10.1149/1.3556609.

[87] M.H. Jang, S.J. Park, D.H. Lim, M.-H. Cho, K.H. Do, D.-H. Ko, H.C. Sohn, Phase change behavior in oxygen-incorporated Ge2Sb2Te5 films, Appl. Phys. Lett. 95 (2009) 012102, https://doi.org/10.1063/1.3168551.

[88] E. Cho, Y. Youn, S. Han, Enhanced amorphous stability of carbon-doped Ge2Sb2Te5: *ab Initio* investigation, Appl. Phys. Lett. 99 (2011) 183501, https://doi.org/10.1063/1.3657139.

[89] K. Bai, T.L. Tan, P.S. Branicio, M.B. Sullivan, Time-temperature-transformation and continuous-heating-transformation diagrams of GeSb2Te4 from nanosecond-long ab initio molecular dynamics simulations, Acta Mater. 121 (2016) 257–265, https://doi.org/10.1016/j.actamat.2016.09.011.

[90] P.S. Branicio, K. Bai, H. Ramanarayan, D.T. Wu, M.B. Sullivan, D.J. Srolovitz, Atomistic insights into the nanosecond long amorphization and crystallization cycle of nanoscale Ge2Sb2 Te5 : an *ab initio* molecular dynamics study, Phys. Rev. Mater. 2 (2018) 043401, https://doi.org/10.1103/PhysRevMaterials.2.043401.

[91] K.B. Borisenko, Y. Chen, D.J.H. Cockayne, S.A. Song, H.S. Jeong, Understanding atomic structures of amorphous C-doped Ge2Sb2Te5 phase-change memory materials, Acta Mater. 59 (2011) 4335–4342, https://doi.org/10.1016/j.actamat.2011.03.057.

[92] K.B. Borisenko, Y. Chen, D.J.H. Cockayne, S.A. Song, H.S. Jeong, Understanding atomic structures of amorphous C-doped Ge2Sb2Te5 phase-change memory materials, Acta Mater. 59 (2011) 4335–4342, https://doi.org/10.1016/j.actamat.2011.03.057.

[93] X. Zhou, L. Wu, Z. Song, F. Rao, M. Zhu, C. Peng, D. Yao, S. Song, B. Liu, S. Feng, Carbon-doped Ge2Sb2Te5 phase change material: a candidate for high-density phase change memory application, Appl. Phys. Lett. 101 (2012) 142104, https://doi.org/10.1063/1.4757137.

[94] M.-C. Jung, Y.M. Lee, K. Kim, Effects of carbon doping on chemical states of amorphous Ge2Sb2Te5, measured with synchrotron radiation, Curr. Appl. Phys. 14 (2014) 1421–1423, https://doi.org/10.1016/j.cap.2014.08.014.

[95] Y. Cheng, D. Cai, Y. Zheng, S. Yan, L. Wu, C. Li, W. Song, T. Xin, S. Lv, R. Huang, H. Lv, Z. Song, S. Feng, Microscopic mechanism of carbon-dopant manipulating device performance in CGeSbTe-based phase change random access memory, ACS Appl. Mater. Interfaces 12 (2020) 23051–23059, https://doi.org/10.1021/acsami.0c02507.

[96] W. Zhou, L. Wu, X. Zhou, F. Rao, Z. Song, D. Yao, W. Yin, S. Song, B. Liu, B. Qian, S. Feng, High thermal stability and low density variation of carbon-doped Ge2Sb2Te5 for phase-change memory application, Appl. Phys. Lett. 105 (2014) 243113, https://doi.org/10.1063/1.4904832.

[97] X. Zhou, M. Xia, F. Rao, L. Wu, X. Li, Z. Song, S. Feng, H. Sun, Understanding phase-change behaviors of carbon-doped Ge_2 Sb_2 Te_5 for phase-change memory application, ACS Appl. Mater. Interfaces 6 (2014) 14207–14214, https://doi.org/10.1021/am503502q.

[98] Q. Hubert, C. Jahan, A. Toffoli, G. Navarro, S. Chandrashekar, P. Noé, V. Sousa, L. Perniola, J.-F. Nodin, A. Persico, S. Maitrejean, A. Roule, E. Henaff, M. Tessaire, P. Zuliani, R. Annunziata, G. Reimbold, G. Pananakakis, B. De Salvo, Carbon-doped Ge_2 Sb_2 Te_5 phase-change memory devices featuring reduced RESET current and power consumption, in: 2012 Proc. Eur. Solid-State Device Res. Conf. ESSDERC, IEEE, Bordeaux, France, 2012, pp. 286–289, https://doi.org/10.1109/ESSDERC.2012.6343389.

[99] Q. Hubert, C. Jahan, A. Toffoli, G. Navarro, S. Chandrashekar, P. Noe, D. Blachier, V. Sousa, L. Perniola, J.-F. Nodin, A. Persico, R. Kies, S. Maitrejean, A. Roule, E. Henaff, M. Tessaire, P. Zuliani, R. Annunziata, G. Pananakakis, G. Reimbold, B. De Salvo, Lowering the Reset current and power consumption of phase-change memories with carbon-doped Ge2Sb2Te5, in: 2012 4th IEEE Int. Mem. Workshop, IEEE, Milan, Italy, 2012, pp. 1–4, https://doi.org/10.1109/IMW.2012.6213683.

[100] T. Li, J. Shen, L. Wu, Z. Song, S. Lv, D. Cai, S. Zhang, T. Guo, S. Song, M. Zhu, Atomic-scale observation of carbon distribution in high-performance carbon-doped Ge_2 Sb_2 Te_5 and its influence on crystallization behavior, J. Phys. Chem. C 123 (2019) 13377–13384, https://doi.org/10.1021/acs.jpcc.9b02098.

[101] X. Zhou, M. Xia, F. Rao, L. Wu, X. Li, Z. Song, S. Feng, H. Sun, Understanding phase-change behaviors of carbon-doped Ge_2 Sb_2 Te_5 for phase-change memory application, ACS Appl. Mater. Interfaces 6 (2014) 14207–14214, https://doi.org/10.1021/am503502q.

[102] R.J. Appleton, Z.D. McClure, D.P. Adams, A. Strachan, Effects of carbon concentration on the local atomic structure of amorphous GST, J. Chem. Phys. 160 (2024) 174702, https://doi.org/10.1063/5.0203532.

[103] T. Li, L. Wu, X. Ji, Y. Zheng, G. Liu, Z. Song, J. Shi, M. Zhu, S. Song, S. Feng, Carbon doping induced Ge local structure change in as-deposited Ge2Sb2Te5 film by EXAFS and Raman spectrum, AIP Adv. 8 (2018) 025201, https://doi.org/10.1063/1.5020614.

[104] R. Qi, F. Sui, R. Huang, S. Song, X. Li, Z. Song, Atomic insight into the BEOL thermal budget on phase transition of phase change memory cells, Appl. Phys. Lett. 123 (2023) 163502, https://doi.org/10.1063/5.0174722.

[105] Y. Yin, D. Niida, K. Ota, H. Sone, S. Hosaka, Scanning electron microscope for in situ study of crystallization of Ge2Sb2Te5 in phase-change memory, Rev. Sci. Instrum. 78 (2007), https://doi.org/10.1063/1.2818804.

[106] Y. Cheng, D. Cai, Y. Zheng, S. Yan, L. Wu, C. Li, W. Song, T. Xin, S. Lv, R. Huang, H. Lv, Z. Song, S. Feng, Microscopic mechanism of carbon-dopant manipulating device performance in CGeSbTe-based phase change random access memory, ACS Appl. Mater. Interfaces 12 (2020) 23051–23059, https://doi.org/10.1021/acsami.0c02507.

[107] Z.T. Song, D.L. Cai, X. Li, L. Wang, Y.F. Chen, H.P. Chen, Q. Wang, Y.P. Zhan, M.H. Ji, High endurance phase change memory chip implemented based on carbon-doped Ge2Sb2Te5 in 40 nm node for embedded application, in: 2018 IEEE Int. Electron Devices Meet. IEDM, IEEE, San Francisco, CA, 2018, pp. 27.5.1–27.5.4, https://doi.org/10.1109/IEDM.2018.8614538.

[108] S. Yan, D. Cai, Y. Xue, Y. Chen, Y. Liu, L. Wu, Z. Song, Investigation on the scaling performances of carbon-doped Ge_2 Sb_2 Te_5 thin films for phase change random access memory in a 40 nm process, Phys. Status Solidi A 216 (2019) 1900439, https://doi.org/10.1002/pssa.201900439.

[109] Y.-G. Liu, Y.-F. Chen, D.-L. Cai, Y.-Y. Lu, L. Wu, S. Yan, Y. Li, J.-J. Lu, L. Yu, Z.-T. Song, High performance of multilevel-cell phase change memory device with good endurance reliability, Semicond. Sci. Technol. 34 (2019) 105019, https://doi.org/10.1088/1361-6641/ab3c93.

[110] Y. Cheng, D. Cai, Y. Zheng, S. Yan, L. Wu, C. Li, W. Song, T. Xin, S. Lv, R. Huang, H. Lv, Z. Song, S. Feng, Microscopic mechanism of carbon-dopant manipulating device performance in CGeSbTe-based phase change random access memory, ACS Appl. Mater. Interfaces 12 (2020) 23051–23059, https://doi.org/10.1021/acsami.0c02507.

[111] P. Arun, A.G. Vedeshwar, N.C. Mehra, Laser-induced crystallization in amorphous films of (C = S, Se, Te), potential optical storage media, J. Phys. Appl. Phys. 32 (1999) 183–190, https://doi.org/10.1088/0022-3727/32/3/001.

[112] Y. Yin, W. Matsuhashi, K. Niiyama, J. Yang, T. Wang, J. Li, Y. Liu, Q. Yu, C–N-codoped Sb2Te3 chalcogenides for reducing writing current of phase-change devices, Appl. Phys. Lett. 117 (2020) 153502, https://doi.org/10.1063/5.0022467.

[113] S. Hwang, J.-S. Oh, T.S. Jung, D. Kim, H. Lim, C. Lee, C.-W. Yang, J.H. Kim, M.-H. Cho, Improvements in thermal stability of Sb_2 Te_3 by modulation of microstructure via carbon incorporation, ACS Appl. Electron. Mater. 3 (2021) 3472–3481, https://doi.org/10.1021/acsaelm.1c00427.
[114] J. Zhang, N. Rong, P. Xu, Y. Xiao, A. Lu, W. Song, S. Song, Z. Song, Y. Liang, L. Wu, The effect of carbon doping on the crystal structure and electrical properties of Sb2Te3, Nanomaterials 13 (2023) 671, https://doi.org/10.3390/nano13040671.
[115] M. Zhang, R. Wang, X. Zou, S. Song, Y. Bao, L. Wu, Z. Song, X. Zhou, Understanding the microstructure evolution of carbon-doped Sb2Te3 phase change material for high thermal stability memory application, Appl. Phys. Lett. 124 (2024) 202101, https://doi.org/10.1063/5.0206244.
[116] M.S. Kim, S.H. Cho, S.K. Hong, J.S. Roh, D.J. Choi, Crystallization characteristics of nitrogen-doped Sb2Te3 films for PRAM application, Ceram. Int. 34 (2008) 1043–1046, https://doi.org/10.1016/j.ceramint.2007.09.078.
[117] Y. Yin, H. Sone, S. Hosaka, Characterization of nitrogen-doped Sb2Te3 films and their application to phase-change memory, J. Appl. Phys. 102 (2007) 064503, https://doi.org/10.1063/1.2778737.
[118] Y. Yin, K. Niiyama, N-O doped Sb_2 Te_3 phase-change materials for high performance artificial synaptic device, in: 2024 IEEE 7th Adv. Inf. Technol. Electron. Autom. Control Conf. IAEAC, IEEE, Chongqing, China, 2024, pp. 1585–1589, https://doi.org/10.1109/IAEAC59436.2024.10503738.
[119] Y. Yin, S. Morioka, S. Kozaki, R. Satoh, S. Hosaka, Oxygen-doped Sb2Te3 for high-performance phase-change memory, Appl. Surf. Sci. 349 (2015) 230–234, https://doi.org/10.1016/j.apsusc.2015.04.229.
[120] T. Zhang, Y. Cheng, Z. Song, B. Liu, S. Feng, X. Han, Z. Zhang, B. Chen, Comparison of the crystallization of Ge–Sb–Te and Si–Sb–Te in a constant-temperature annealing process, Scr. Mater. 58 (2008) 977–980, https://doi.org/10.1016/j.scriptamat.2008.01.048.
[121] K. Ren, F. Rao, Z. Song, L. Wu, X. Zhou, B. Liu, S. Feng, W. Xi, B. Chen, Phase change memory cell using Si_2 Sb_2 Te_3 material, Jpn. J. Appl. Phys. 49 (2010) 080212, https://doi.org/10.1143/JJAP.49.080212.
[122] B. Qiao, J. Feng, Y. Lai, Y. Cai, Y. Lin, T. Tang, B. Cai, B. Chen, Si–sb–te films for phase-change random access memory, Semicond. Sci. Technol. 21 (2006) 1073–1076, https://doi.org/10.1088/0268-1242/21/8/016.
[123] F. Rao, Z. Song, K. Ren, X. Zhou, Y. Cheng, L. Wu, B. Liu, Si–Sb–Te materials for phase change memory applications, Nanotechnology 22 (2011) 145702, https://doi.org/10.1088/0957-4484/22/14/145702.
[124] H.Y. Cheng, Z.L. Liu, A. Majumdar, A. Grun, A. Ray, J. Su, M.J. Rasch, F. Carta, L. Gignac, C. Lavoie, C.W. Cheng, M.B. Sky, H.L. Lung, State-Independent Low Resistance Drift SiSbTe Phase Change Memory for Analog In-Memory Computing Applications, in: 2024, IEEE Symp. VLSI Technol. Circuits VLSI Technol. Circuits, IEEE, Honolulu, HI, USA, 2024, pp. 1–2, https://doi.org/10.1109/VLSITechnologyandCir46783.2024.10631376.
[125] Y. Cheng, Y. Zheng, Z. Song, Reversible switching in bicontinuous structure for phase change random access memory application, Nanoscale 13 (2021) 4678–4684, https://doi.org/10.1039/D0NR09139A.
[126] X. Li, F. Rao, Z. Song, K. Ren, W. Liu, Z. Sun, Experimental and theoretical study of silicon-doped Sb2Te3 thin films: structure and phase stability, Appl. Surf. Sci. 257 (2011) 4566–4568, https://doi.org/10.1016/j.apsusc.2010.12.017.
[127] X.-P. Wang, N.-K. Chen, X.-B. Li, Y. Cheng, X.Q. Liu, M.-J. Xia, Z.T. Song, X.D. Han, S.B. Zhang, H.-B. Sun, Role of the nano amorphous interface in the crystallization of Sb2Te3 towards non-volatile phase change memory: insights from first principles, Phys. Chem. Chem. Phys. 16 (2014) 10810, https://doi.org/10.1039/c3cp55476g.
[128] H.Y. Cheng, Z.L. Liu, A. Majumdar, A. Grun, A. Ray, J. Su, M.J. Rasch, F. Carta, L. Gignac, C. Lavoie, C.W. Cheng, M.B. Sky, H.L. Lung, State-Independent Low Resistance Drift SiSbTe Phase Change Memory for Analog In-Memory Computing Applications, in: 2024, IEEE Symp. VLSI Technol. Circuits VLSI Technol. Circuits, 2024, pp. 1–2, https://doi.org/10.1109/VLSITechnologyandCir46783.2024.10631376.
[129] Z. Song, R. Wang, Y. Xue, S. Song, The "gene" of reversible phase transformation of phase change materials: octahedral motif, Nano Res. 15 (2022) 765–772, https://doi.org/10.1007/s12274-021-3570-1.
[130] Y. Xue, Y. Cheng, Y. Zheng, S. Yan, W. Song, S. Lv, S. Song, Z. Song, Phase change memory based on Ta–Sb–Te alloy –Towards a universal memory, Mater. Today Phys. 15 (2020) 100266, https://doi.org/10.1016/j.mtphys.2020.100266.
[131] J. Zhao, W.-X. Song, T. Xin, Z. Song, Rules of hierarchical melt and coordinate bond to design crystallization in doped phase change materials, Nat. Commun. 12 (2021) 6473, https://doi.org/10.1038/s41467-021-26696-9.
[132] F. Rao, K. Ding, Y. Zhou, Y. Zheng, M. Xia, S. Lv, Z. Song, S. Feng, I. Ronneberger, R. Mazzarello, W. Zhang, E. Ma, Reducing the stochasticity of crystal nucleation to enable subnanosecond memory writing, Science 358 (2017) 1423–1427, https://doi.org/10.1126/science.aao3212.
[133] R. Wang, Z. Song, W. Song, T. Xin, S. Lv, S. Song, J. Liu, Phase-change memory based on matched Ge-Te, Sb-Te, and In-Te octahedrons: improved electrical performances and robust thermal stability, InfoMat 3 (2021) 1008–1015.